

*Unclassified*

SECURITY CLASSIFICATION OF THIS PAGE

REF ID: A7481  
2

REPORT DOCUMENTATION PAGE

TIC

10. RESTRICTIVE MARKINGS

3. DISTRIBUTION/AVAILABILITY OF REPORT

Approved for public release;  
distribution unlimited

5. MONITORING ORGANIZATION REPORT NUMBER(S)

AFOSR-TR- 90-0603

4. PERFORMING ORGANIZATION REPORT NUMBER(S)

6a. NAME OF PERFORMING ORGANIZATION  
Smithsonian Institution  
Astrophysical Observatory

6b. OFFICE SYMBOL  
(If applicable)

7a. NAME OF MONITORING ORGANIZATION

Air Force Office of Scientific Research

6c. ADDRESS (City, State, and ZIP Code)

60 Garden St.  
Cambridge, MA 02138

7b. ADDRESS (City, State, and ZIP Code)

Bldg 41C  
Bolling AFB,  
D.C. 20332-6448

8a. NAME OF FUNDING/SPONSORING  
ORGANIZATION

AFOSR

8b. OFFICE SYMBOL  
(If applicable)

NP

9. PROCUREMENT INSTRUMENT IDENTIFICATION NUMBER

AFOSR-B6-0103

8c. ADDRESS (City, State, and ZIP Code)

Building 410  
Bolling AFB, DC 20332-6448

10. SOURCE OF FUNDING NUMBERS

PROGRAM ELEMENT NO.	PROJECT NO.	TASK NO.	WORK UNIT ACCESSION NO.
611021F	2311	A1	

11. TITLE (Include Security Classification)

High Resolution Optical Imaging Through the Atmosphere

12. PERSONAL AUTHOR(S)

R. W. Noyes; P. Nisenson; R. V. Stachnik; C. Papaliolios; W.

13a. TYPE OF REPORT  
FINAL

13b. TIME COVERED

FROM 2/1/86 TO 9/30/89

14. DATE OF REPORT (Year, Month, Day)

12/28/89

15. PAGE COUNT

12

16. SUPPLEMENTARY NOTATION

COSATI CODES		
FIELD	GROUP	SUB-GROUP
	C3.01	

16. SUBJECT TERMS (Continue on reverse if necessary and identify by block number)

optical imaging; active optics; solar speckle  
imaging; stellar speckle imaging

17. ABSTRACT (Continue on reverse if necessary and identify by block number)

This program has concentrated on three major areas: the application of high angular resolution image reconstruction techniques to the reconstruction of solar surface features; speckle imaging of a wide range of astronomical sources; and the implementation of adaptive optics for faint object imaging. In this project, we have made substantial modifications to a technique for reconstruction of high resolution images from single short exposure solar frames, blind iterative deconvolution (IDC). We have been testing these improvements using numerical simulation data. Analysis of speckle data of the supernova SN1987A has detected a new bright source, 0.9 arcseconds south of the SN, as well as substantial structure in the region surrounding the SN. We also have new results on several Young Stellar Objects and supergiants. In the area of adaptive optics, an AOA wavefront sensor has been set up and tested using an image intensifier which increases its sensitivity by three orders of magnitude. Faint object image active tilt correction has also been tested with some important enhancements, including new highly linear and sensitive CCD quad cells developed by Cal Tech and Tektronix, and an off-the-shelf high-speed 2-D tilting mirror with greatly improved specifications. The effects of only partially correcting atmospheric turbulence have been theoretically analyzed and numerically simulated.

20. DISTRIBUTION/AVAILABILITY OF ABSTRACT

UNCLASSIFIED/UNLIMITED  SAME AS RPT.  DTC USERS

21. ABSTRACT SECURITY CLASSIFICATION

Unclassified

22a. NAME OF RESPONSIBLE INDIVIDUAL

Henry Padoksi

22b. TELEPHONE (Include Area Code)

202-767-4906

22c. OFFICE SYMBOL

NP

DD FORM 1473, 84 MAR

83 APR edition may be used until exhausted.

All other editions are obsolete.

SECURITY CLASSIFICATION OF THIS PAGE

Unclassified

## Abstract

This program has concentrated on three major areas: the application of high angular resolution image reconstruction techniques to the reconstruction of solar surface features; speckle imaging of a wide range of astronomical sources; and the implementation of adaptive optics for faint object imaging. In this project, we have made substantial modifications to a technique for reconstruction of high resolution images from single short exposure solar frames, blind iterative deconvolution (IDC). We have been testing these improvements using numerical simulation data. Analysis of speckle data of the supernova SN1987A has detected a new bright source, 0.9 arcseconds south of the SN, as well as substantial structure in the region surrounding the SN. We also have new results on several Young Stellar Objects and supergiants. In the area of adaptive optics, an AOA wavefront sensor has been set up and tested using an image intensifier which increases its sensitivity by three orders of magnitude. Faint object image active tilt correction has also been tested with some important enhancements, including new highly linear and sensitive CCD quad cells developed by Cal Tech and Tektronix, and an off-the-shelf high speed 2-D tilting mirror with greatly improved specifications. The effects of only partially correcting atmospheric turbulence have been theoretically analyzed and numerically simulated.

## I. SOLAR IMAGING

Extensive experiments performed in the area of solar speckle imaging have proven to be limited in the accuracy of the reconstructions due to the long sequences of data required for diffraction limited recovery. Solar surface features appear to evolve on time scales substantially shorter than the time required to take a long enough series of frames with a CCD camera. This problem was demonstrated through experiments which tested reconstruction algorithms using computer generated simulation data, and by processing shorter sets of real solar data. The non-time-varying simulations recovered the highest frequency information with excellent accuracy. In the real data, short data sets (20 frames @ 2 frames/sec) recovered artifact free but un converged images, while longer data sets (100 frames) produced fringe like artifacts in the reconstructions, apparently due to

or	
SI	<input checked="" type="checkbox"/>
d	<input type="checkbox"/>
REMARKS	
Key Codes	
Mod / or Special	
DATA	
A-1	

evolution in the solar features. This rapid evolution of high resolution features has recently been documented in Skylab solar data sequences, and in sequences of solar frames recorded under optimal seeing conditions at the La Palma solar telescope.

Obviously, one possible approach to solving these problems is a more rapid recording of data. However, obtaining long enough sequences under good conditions is difficult and could not be used in any sort of routine observing mode. In this program, we have directed our efforts toward the development of algorithms which could reconstruct images from much shorter sequences of data. In solar imaging, the signal-to-noise of each frame is very high, due to the high light levels, and this is the major requirement for the successful application of Blind Iterative Deconvolution techniques.

### **Blind Iterative Deconvolution**

Blind Iterative deconvolution (ID) (Ayers and Dainty, 1988) combines iterative techniques such as those developed for phase retrieval (Fienup, 1978) with blind deconvolution (Lane and Bates, 1987). One starts with an image which is degraded by some blurring function. A necessary condition for the algorithm to work is that the blurring function be constant over the entire image field to be restored (stationarity). It is also assumed that the degradation is a linear operation. The general approach is then to find a pair of functions whose convolution gives the input image within a set of physical constraints, such as positivity of the two convolved functions or the signal-to-noise ratio in the Fourier transform (FT). While it has not been proven that the derived functions are unique, complicated images appear to converge on only one sensible solution.

A flow diagram for the technique is given in figure 1. One starts with a degraded image and an initial estimate of the point spread function (PSF). The initial PSF can be completely random, however the number of cycles of iteration required to converge on an acceptable answer is highly dependant on how close the first estimate of the PSF is to the actual PSF. Both inputs are Fourier transformed and a deconvolution is performed by dividing the FT of the image by the FT of the PSF. Constraints are applied to the ratio based on estimated signal-to-noise ratios. The result is transformed back to image space and the positivity and support constraints are applied (the image support is defined as the region in which the image is non-zero). The negatives in the image are summed and the pixels with negative values are set to zero. The negatives are then uniformly subtracted within the support region in order to preserve the total power in the image. The sum of the negatives is also used as a diagnostic of convergence. The FT of the original degraded image is then deconvolved by the FT of the image obtained from the previous iteration. Fourier plane constraints are applied and the result is transformed back to image space. Again, positivity and the support constraint are enforced. The result is a new estimate of the PSF. The iteration continues until some concluding criterion is reached. Either a limit to the number of cycles, or the level of residual negatives in the image, or some other image quality criterion may determine the stopping point. After examination of the output image and PSF, the results may be fed back into the loop for continued iterations.

There are a number of parameters which must be chosen in order to ensure convergence and an optimum result. Probably the most important are estimates of the signal-to-noise ratio in the data and the range of spatial frequencies over which the image recovery operation is performed. A low pass filter is applied in frequency space after each cycle and then its inverse filter is applied before each deconvolution. The extent of this filter is adjusted for the signal-to-noise ratio in the image and the PSF.

## Reconstructions with ID

The work on ID already undertaken at CfA has produced an algorithm that has been tested with computer simulations and also applied to some real data. Results of the simulations are shown in Figs. 2 and 3. Fig. 2a shows the input diffraction limited image of 8 point sources, the bottom right-hand "point" being two unresolved points. This image was convolved with the PSF in Fig. 2b to produce the input image to be deconvolved with ID shown in Fig. 2c. The starting guess for the PSF (Fig. 2d) used to perform the first cycle of ID was a gaussian with random noise and a half power width with approximately the same radius as the input image. In most real situations, there is usually some reasonable estimate of the PSF which, when used as a first guess, should improve the rate of convergence. Here, a random PSF was used to demonstrate the dramatic evolution of the reconstructed PSF towards the actual diffraction limited PSF, despite the poor starting estimate. The image and PSF obtained from ID after 20 cycles are shown in Figs. 3a and 3b, respectively. The major features present in the diffraction limited image and PSF have been reconstructed, however further iterations lead to a considerable improvement in the reconstructions. Figs. 3c and 3d show the image and PSF reconstructions after 180 cycles of ID. Comparison of these results with Figs. 2a and 2b show a dramatic recovery of both the morphology and intensities present in the diffraction limited image and PSF.

These initial computer simulations have produced highly encouraging results. However, detailed characterization of the effects of noise and the robustness of the convergence under variations in reconstruction parameters have not been rigorously investigated. For ID or any deconvolution method to be a useful tool, it must be rigorously characterized with both simulations and real data.

Some initial attempts have been made to use the technique on real x-ray and optical CCD data. Figs. 4a-c show the results of processing a 128x128 pixel Einstein image of

SNR 0540-69.3. Fig. 4a is a contour plot of the input image (the input image had one smoothing pass). Fig. 4b shows the result from ID after only 10 cycles of iteration. There has obviously been a great increase in the intensity and sharpening of the central source. Structure around the source is evident at scales of about 10 arcseconds. Fig. 4c shows the recovered PSF. Additional cycles of ID made almost no change in the reconstruction, indicating a stable solution for the chosen parameters. It's possible that other parameters, such as allowing the signal-to-noise ratio a greater latitude might produce some additional sharpening. However this result is already very promising. It will be interesting to compare these results to optical images processed in a similar manner, where extended structure is known to be on the same scale as the recovered features.

Figs. 5a-c show results of ID processing on CCD images of supernova SN1987A recorded at the CTIO 4-meter telescope in March, 1989 (Heathcote, 1989). 5a shows the original image of the supernova, its two companions, and the suspected optical echo. The wide companion is separated by 2.9 arcseconds from the SN. 5b is the ID reconstruction, again after only 10 cycles of processing and 5c shows the derived PSF. Clearly the image has been sharpened and both the stars and the echo are now well resolved. These results demonstrate the power of the technique, and show that one obtains rapid convergence if a good initial estimate of PSF is available.

We are currently testing approaches to adding what may be a still more powerful convergence constraint. If a series of short exposure images is recorded where the object remains constant but the degrading atmosphere changes, then each frame should converge to the same image, but with very different PSF's. Forcing commonality between separate results from two or more independent iterations should prove to have an important effect on convergence properties.

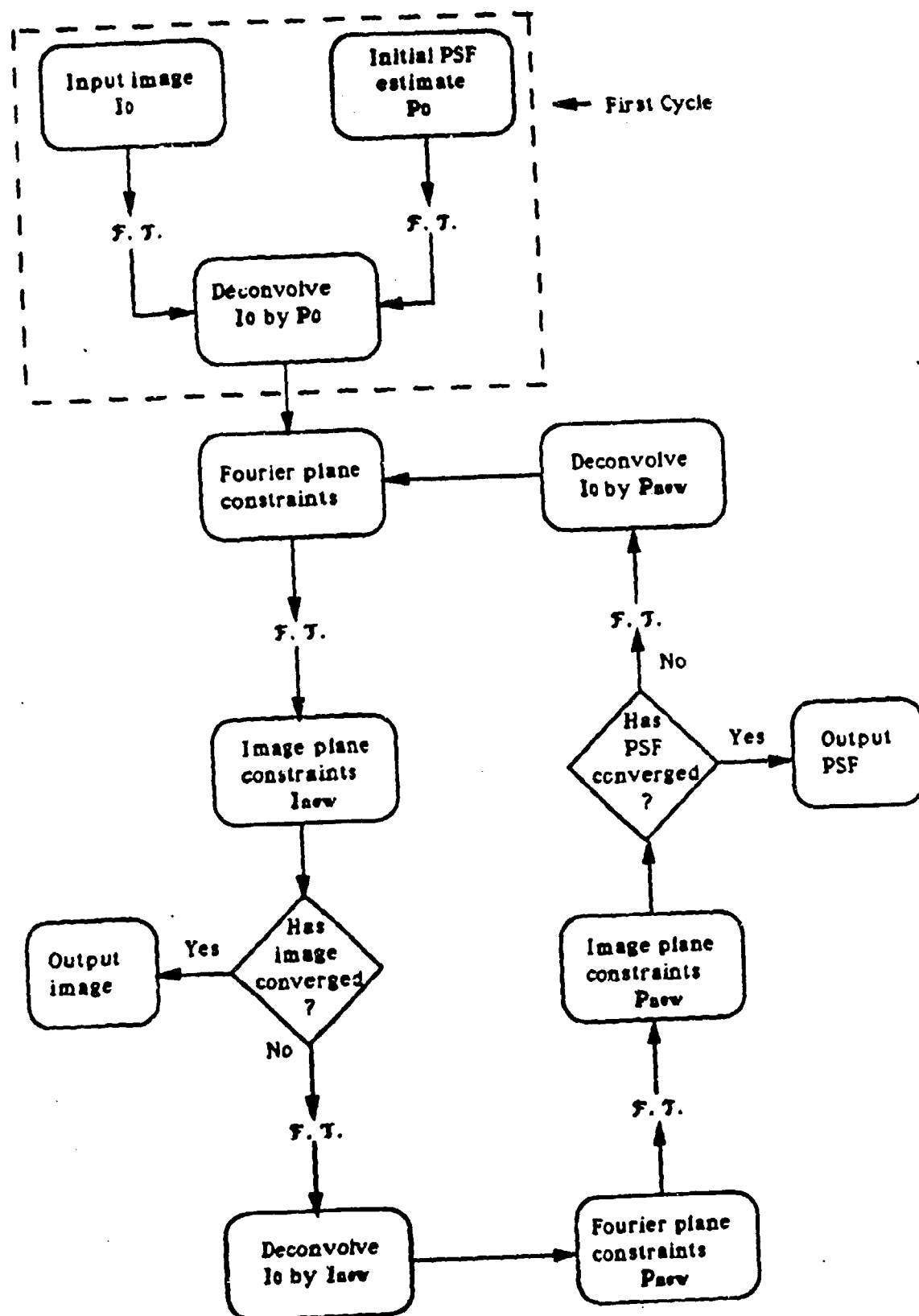


Fig. 1 Flow Diagram of the Iterative Deconvolution Algorithm

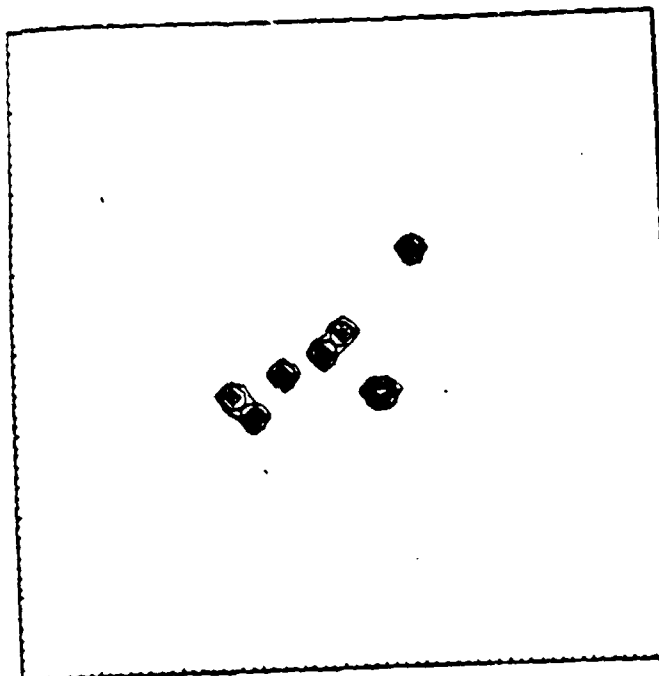


Fig. 2a The diffraction limited image of 8 point sources 2 of which are unresolved.

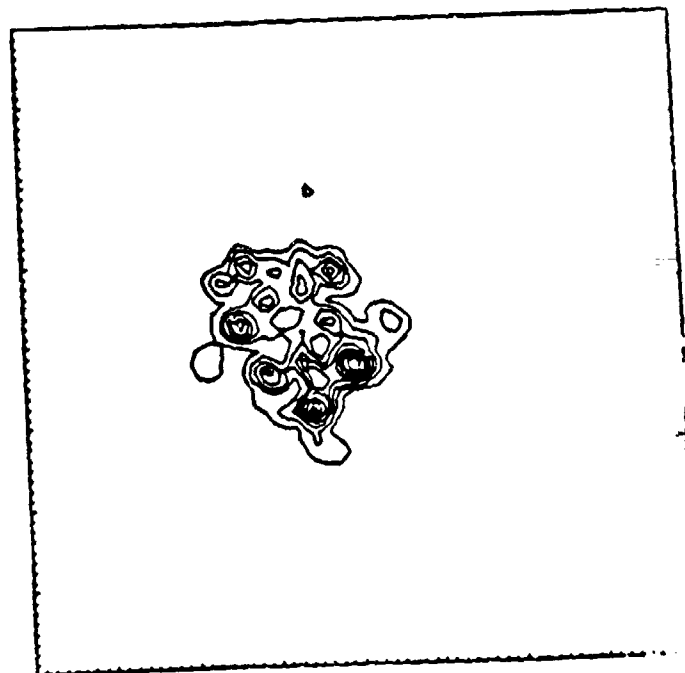


Fig. 2b The diffraction limited point spread function (PSF)

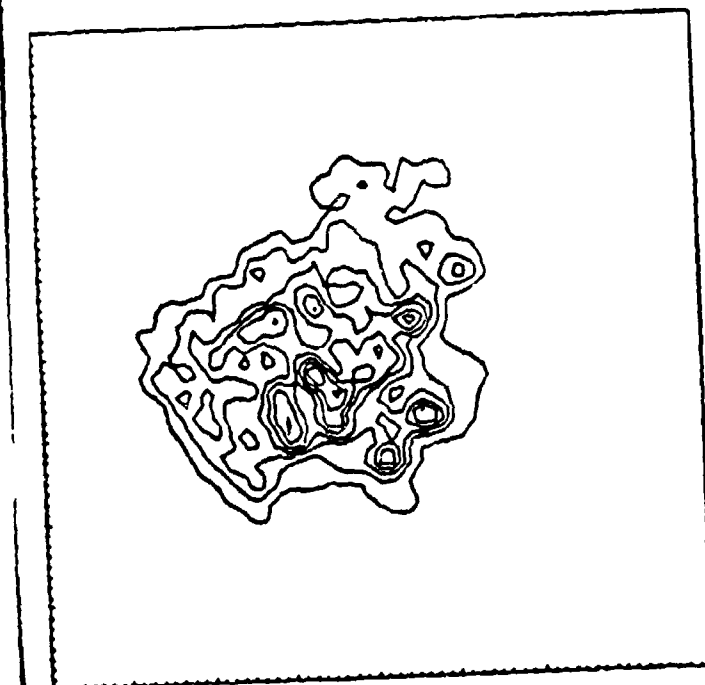


Fig. 2c The input image, the convolution of Fig. 2a with Fig. 2b.

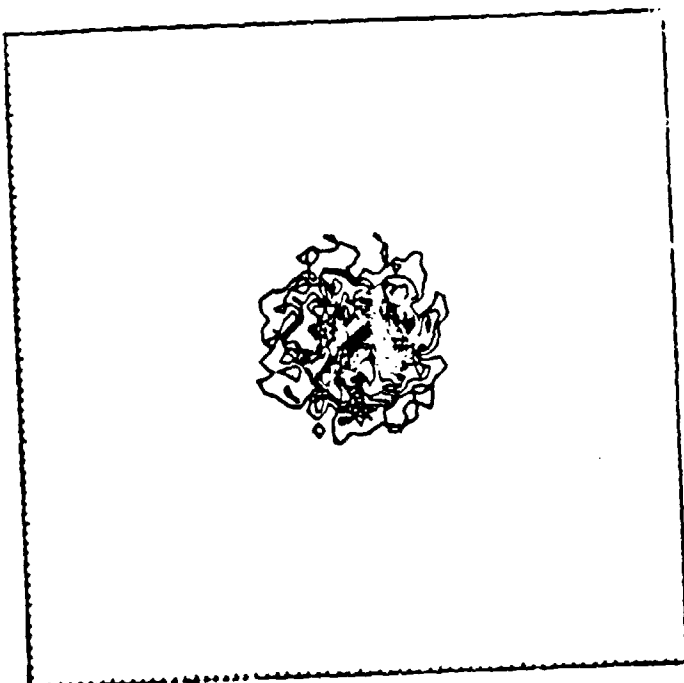


Fig. 2d The starting PSF for the first cycle of iterative deconvolution.

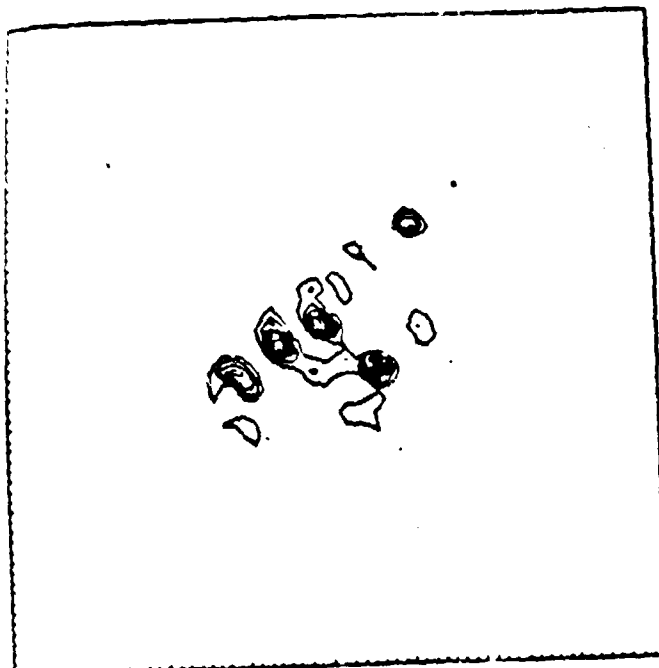


Fig. 3a The reconstruction of the image after 20 cycles of iterative deconvolution.

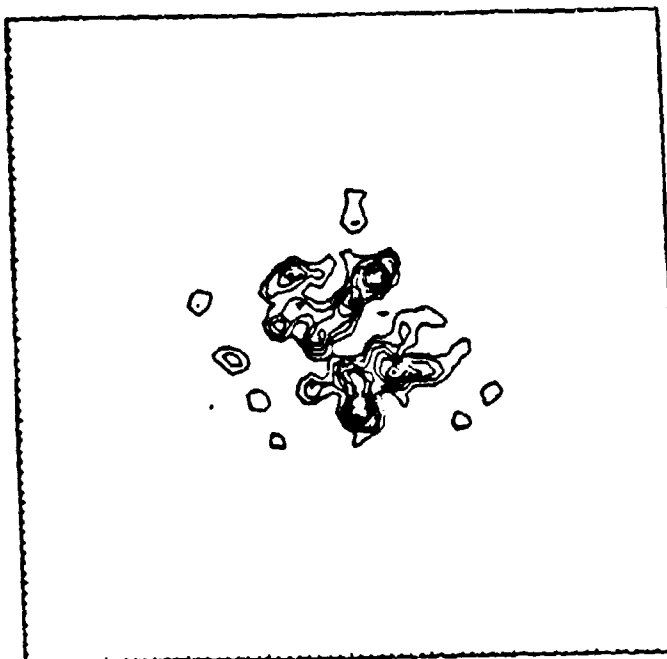


Fig. 3b The reconstruction of the PSF after 20 cycles of iterative deconvolution.

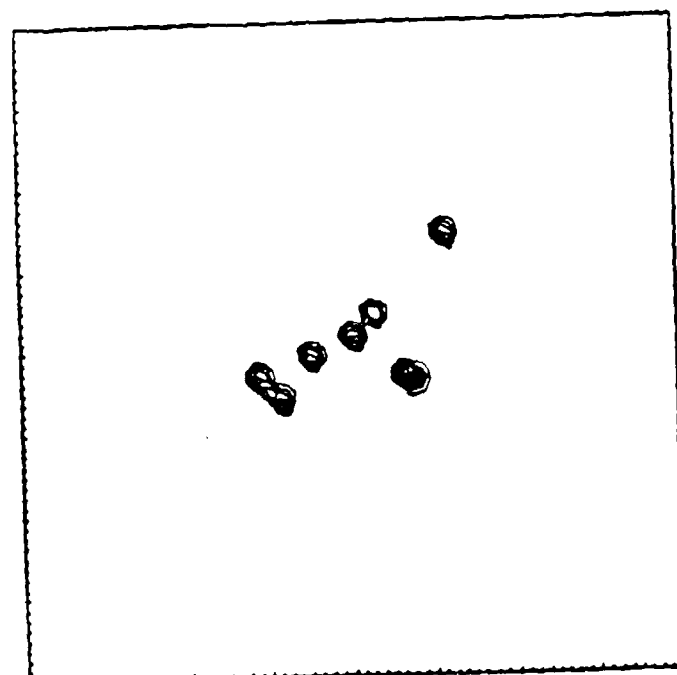


Fig. 3c The reconstruction of the image after 180 cycles of iterative deconvolution.

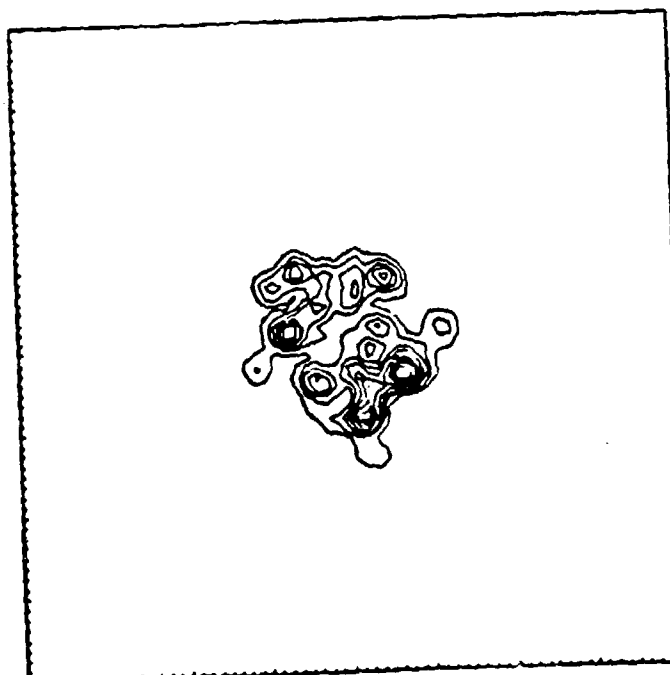
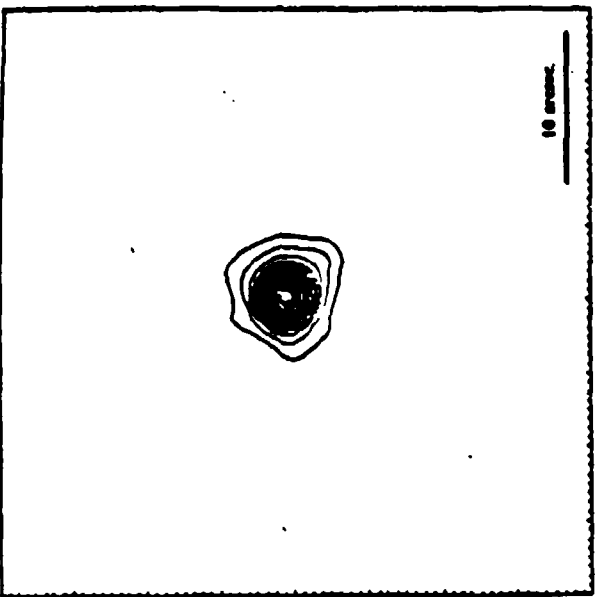
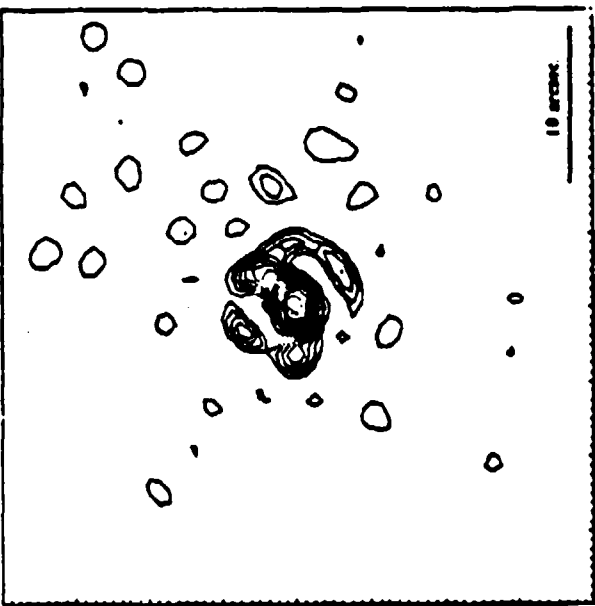


Fig. 3d The reconstruction of the PSF after 180 cycles of iterative deconvolution.



**Fig. 4a** An X-ray image of SNR0540 taken with the Einstein Observatory.



**Fig. 4b** The reconstruction of SNR0540 after 10 cycles of ID.

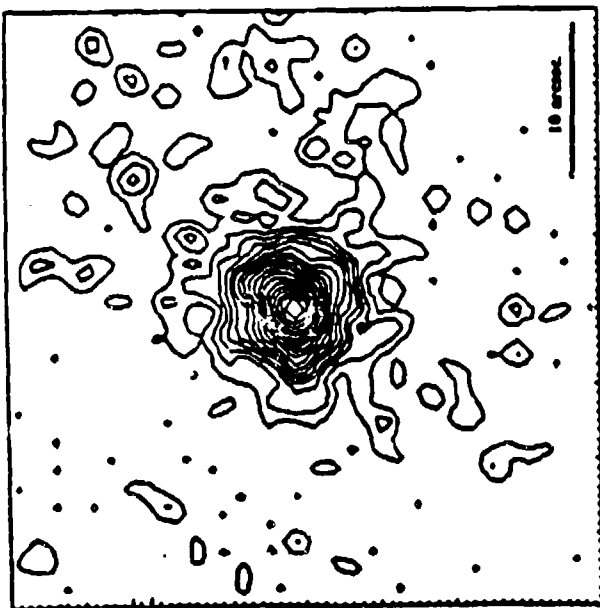


**Fig. 4c** The reconstruction of the PSF after 10 cycles of ID.

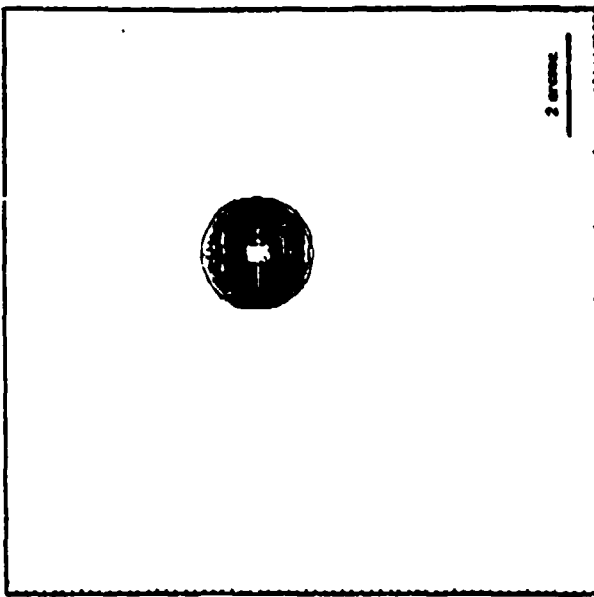


**Fig. 5a** A CCD image of SN1987A recorded in March 1989 at the CTIO 4m. telescope.

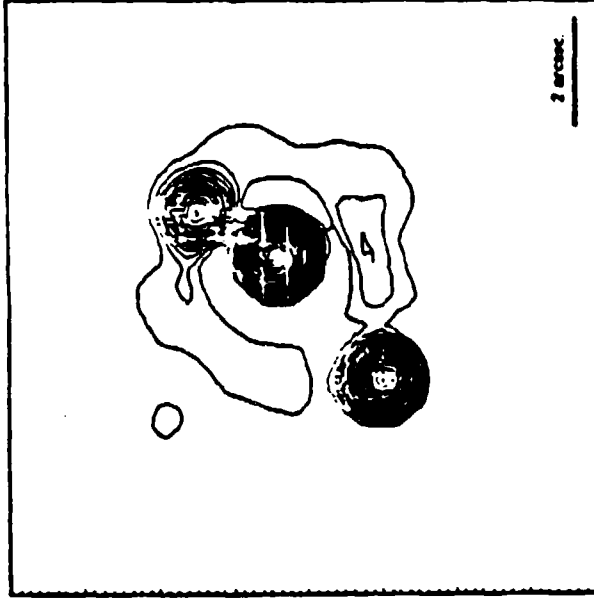


**Fig. 5b** The reconstruction of SN1987A after 10 cycles of ID.

**Fig. 5c** The reconstruction of the PSF after 10 cycles of ID.

In the solar imaging problem, we had only limited success using standard speckle image reconstruction techniques for reconstructing high resolution solar images, due to the large number of frames required to give good signal-to-noise ratio images. With the IDC technique, only a few frames are required, so the stability problem is not an issue. Other questions that remain are the problem of isoplanicity (over how large an angle is the atmospheric PSF stationary?), and do the boundaries of the image caused by the finite size of the detector cause degradation? Some of the techniques we have used for speckle will play an important role, particularly "detrending", where edge effects are reduced by subtraction of a low-pass filtered version of the image before processing. Also, what are the effects of using an imperfect detector? The isoplanatic problem and the detector effects can only be tested with real data, though we are able to add simple forms of noise to the simulations, while the boundary problem may be explored with simulations.

Tests of the IDC approach are continuing with CCD data recorded at the Sacramento Peak Solar Observatory and data recorded by a group from Lockheed who observed using the Swedish solar telescope at La Palma . The atmospheric conditions are sufficiently good so that some individual frames are nearly diffraction limited. By obtaining sequences of frames where the seeing is very good and then degrades, one can compare the results to the very good frames, giving a form of "ground truth" for testing the IDC reconstruction process. Processing several separate degraded frames and comparing the results to each other and the best frames is also important.

We believe that ID could produce very good solar physics. It could allow long sequences of frames to be corrected, and mosaics of much larger fields than the isoplanatic patch could be synthesized from overlapping reconstructions of small areas. It could also be applied to data recorded at telescopes with large apertures, where the atmosphere will always have a substantial degrading effect.

## II. ADAPTIVE OPTICS

### Star-Tracker

A new adaptive optics laboratory has been equipped and is now in operation. Initially it was used to evaluate the performance of an experimental "star-tracker", which consists of a position sensor, a processor and a simple actuator. These components form a closed loop control system. The position of an attenuated laser spot is monitored by a quad-cell and the resulting four voltages are read by a Macintosh II computer. A Kalman filter has been implemented on the Macintosh II which predicts the position of the laser spot from its previous displacements across the quad-cell. From the output of this Kalman filter, a control voltage (ranging from 0 to +10 volts) is derived which is then used to control the piezoelectric actuators and return the laser spot to the center of the quad-cell. The position of the laser spot is controlled by a gimbal mounted mirror which can be tilted about two perpendicular axes by two piezostatic actuators. However, as the actuators produce their maximum displacement with a driving voltage of 1000 volts an amplifier has been constructed to multiply the control voltage by a factor of one hundred before it is applied to the actuators. The Mac II is also used to produce atmospheric simulation error signals which can be fed to a second active mirror in the system. These errors are independent and random, with statistics matching an atmospheric model. The correction system then performs its operation and the residuals are measured. This allows a full test and optimization of the tracking system in the lab, over a realistic set of conditions, at a range of light levels, time constants, and atmospheric variances.

Two new hardware components should aid in the implementation of faint object high speed active guiding. Special CCD quad cells have been developed by a collaboration between groups at Tektronix, Cal Tech, and Johns Hopkins University. These cells have

very high quantum efficiency, very low readout noise (a few electrons) and can be read out at kilohertz rates. They appear to be ideal for detection of image centroids at the low light levels, required for astronomical rapid guiding and interferometry. Cal Tech is making some of these chips available to us, and Johns Hopkins is providing designs for mounting and cooling the chips. We have also located a high speed tilt mirror which should have greatly improved performance compared to the Burleigh mirrors which we have been trying to use for this purpose. The mirror was designed by a German company, Physike Corp., for use by the European Southern Observatory. There are a few specifications that we are still checking on (vibration and piston motion) but from what we have already learned, this mirror appears to have more than adequate characteristics for high speed image tracking and correction.

#### **AOA Wavefront Sensor**

A wavefront sensor, which uses the Hartmann test to determine atmospheric wavefront distortions, has been constructed and demonstrated by Adaptive Optics Associates (AOA) under the control of their MassComp computer. AOA then undertook to port the controlling software from MassComp Unix to VMS on our Dec MicroVax. Unfortunately their experience with VMS was very limited and they were over optimistic in the assessment of their ability to translate the operational environment from Unix to VMS. Therefore, it was decided to install a Unix operating system on the MicroVax. Once this was completed the graphics, data transfer, and control software were installed with little difficulty and A.O.A. The wavefront sensor has now been delivered and initial tests have been performed with it. The next step will be to produce a set of controlled aberrated wavefronts to test our approach of computational estimation and correction. We will then extend these test by interfacing the sensor to our atmospheric simulator and photon camera.

This will allow a full test of our partial atmospheric correction and adaptive optics- speckle imaging applications.

We have completed the implementation of improved software on the Microvax which controls the AOA wavefront sensor. The use of correlation techniques to locate and apply the array of subapertures has proven to be very effective. With the software, as delivered by AOA, determination of the positions of the subapertures was extremely erratic. Since this is a critical element in the operation of the sensor, testing could not be continued until this problem was solved. There were numerous other problems with the control and display software, some of them due to the conversion of the software from a Masscomp computer to the Vax, and some fundamental to the software design. The software is finally in sufficiently good shape to allow more extensive laboratory tests of faint object wavefront sensing and correction. Problems with the three stage image intensifier , needed to allow the sensor to work at photon counting levels for astronomical sources, were finally corrected during this reporting period. Extensive tests of the low light mode of operation have not yet been performed.

### Partial Atmospheric Correction Analysis

Wavefront sensors such as the AOA system we have purchased are expensive and technologically complicated, requiring massive parallel computation and extensive electronic control systems for their operation. A large telescope under typical seeing conditions will have several hundred to thousands of correlation areas across its pupil, requiring an equal number of correction channels in an adaptive optics system if full correction is to be obtained. Our system has only 37 correction elements, so it could only fully correct a very small telescope. However, we have performed numerical experiments and analyses to determine the effectiveness of using a corrector with many fewer elements

than the number of correlation areas in the pupil. The results show (Nisenson and Barakat, 1987) that even a very limited number of elements can produce a surprisingly large improvement in the atmospheric "seeing". The wavefront sensor, in effect, corrects only the lower spatial frequencies, leaving a residual high frequency background, but concentrating the energy in the system point spread function. Correcting only low spatial frequencies allows light collection over larger regions in the pupil and these regions have a commensurately longer time constant. This allow the system to operate to substantially fainter magnitude limits. The detailed results of this analysis are included as an appendix in this report.

### III. SPECKLE IMAGING ASTRONOMY

#### The New PAPA 2-d Photon Counting Detector

A new version of the PAPA 2-dimensional photon counting camera has been developed, in collaboration with four groups at other institutions who are involved with speckle imaging and long-baseline interferometry. Five cameras have been built with greatly improved characteristics compared to the original PAPA, which was built with funding from AFOSR. The primary advantages of the new PAPA are increased quantum efficiency (>10 %), higher maximum count rate (>1 Mhz), a much lower error rate, and much better thermal and mechanical stability. The new camera also has 11 bit by 11 bit resolution (2048x2048 pixels) compared to the 256x256 resolution of the old camera. The increased sensitivity and speed of the new camera allows us to obtain enhanced resolution imaging of the SN and its circumstellar environment, despite their overall decline in brightness.

## Observations of SN1987A

High angular resolution observations of SN1987A (SN) have provided valuable data that contribute to the understanding of this extraordinary astrophysical event. Using speckle interferometric techniques, it is possible to overcome the resolution limits imposed by atmospheric turbulence and observe, in some detail, the morphology of the SN and its environment. A wide variety of other techniques such as spectroscopy, photometry, polarimetry, X-ray and gamma-ray observations are providing an extensive data base that, combined with the high angular resolution measurements will give a detailed understanding of the mechanisms and dynamics of supernovae, testing the validity of theoretical models.

Speckle observations at CTIO in March-April revealed the presence of a second bright source separated by only 60 mas from the SN, and within a factor of 10 of its brightness. Furthermore, analysis of data acquired in March-April along with data from two other runs in May-June, and November, 1987, provided measurements of the apparent diameter of the SN at several wavelengths. Most recently, data recorded in March and April of 1988 show evidence for strong asymmetries in the expanding SN shell, with the major axis of the asymmetry in the same direction as the measured axis of polarization, as well as the direction of earlier detected bright 2nd source.

Diameter measurements were made by fitting the integrated power spectra obtained from the speckle process to the power spectrum of a uniform disk (an Airy disk). Accurate fitting allows diameter estimates at scales well below the "diffraction limit" of the telescope, to accuracies of a few milliarcseconds.

While measurements of equivalent precision have not previously been demonstrated using speckle techniques, the validity of our results has been supported by laboratory

simulations and measurements of stars whose diameters have been determined by other techniques. Results show that diameters measured in H $\alpha$  are in good agreement with predictions based on measurements of the velocity from the H $\alpha$  trough. Measurements in the earliest months after the explosion showed a surprisingly large diameter in the continuum, but results in the later months gave results closer to predicted scales. We have set up an extended observing program in collaboration with scientists at CTIO, so that speckle data is being acquired on once-a-month basis. Latest results indicate a substantial asymmetry in the supernova shell, with an axis aligned in the direction of the measured polarization. As the supernova expands, its details should be observable with an ever increasing degree of detail. Our technique appears to be providing a unique window on this one-of-a-kind object. The success of our measurements to better than 1 mas precision may also provide a tool for many other scientific problems which was previously thought only possible with long baseline interferometers, but at much fainter magnitude limits than would be achievable with an interferometer.

Reduction of speckle data recorded on November 28, 1988, December 20, 1988, and January 20, 1989 show the existence of a bright source near SN1987A (IAU Circulars # 4749 and 4752). Observations performed with the CTIO 4-meter telescope, the PAPA detector, and speckle image reconstruction techniques show a source located at P.A. 200 (+/- 5) degrees for all observations. Preliminary estimates of the magnitude differences from the SN (551 nm) and angular separations were: 3.3 (+/- 0.2) magnitudes and 0.85 (+/- 0.05) arcsec (November 28); 2.6 (+/- 0.2) and 0.85 (+/- 0.05) (December 20); and 2.1 (+/- 0.2) magnitudes and 0.95 (+/- 0.05) arcsec (January 20). The separation and position angle of this source is consistent with the position of the compact blob reported by Allen et al (IAU circular # 4747). It is also consistent with a position predicted for uniform motion of the bright source which was detected using speckle techniques on April 1, 1987 (IAU circular # 4382 ) and by Matcher et al on April 15, 1987 (IAU Circular # 4413). We note

that the brightness of this source is consistent with the rate of decay of the supernova, so if this is the same object detected almost two years ago, its energy source may well be Cobalt-56 decay.

We were also able to detect star 2 separated by 2.8 arcseconds from the SN with a magnitude difference of about 3 (at 551 nm) and position angle of 315 (+/- 5) degrees and star 3 is just barely detectable at a separation of 1.7 arcseconds and position angle 110 degrees. We did not detect any feature to the north of the SN, as suggested by Allen's long-slit spectral measurements. Initial reductions of CCD data recorded at the prime focus of the CTIO 4-meter show possible confirmation of these detections.

It should continue to be extremely interesting to observe the SN as it evolves, in particular when it allows a first close look at the formation of an SNR. We will look for scattering sources and possible evidence for early signs of synchrotron radiation. If the rapidly spinning pulsar is actually in the center of the SN, as early observations suggest, than speckle-polarization experiments may be able to detect its effect on the surrounding medium. Finally, SN1987A has provided many unexpected results during the past 3 years with behavior which has not been predicted by existing SN models. We believe that this is a compelling reason for continued careful monitoring with all available techniques.

### **Young Stellar Objects**

Results from our study of several YSO's show a number of stars with extended disk-like structures. Observations of DG Tau at several wavelengths including 6308 Å [OI], the adjacent continuum and H $\alpha$  reveal extended asymmetric structure at angular scales larger than 0.3 arcsecond. This asymmetry is located along NW-SE direction and is aligned with the direction of the observed jet. An extended halo around Walker 90 was also discovered. The halo is elongated in a SE-NW direction and is almost perpendicular to

the measured polarization angle. Results obtained from fitting a power law model to the intensity profile of the extended halo indicates the presence of a flared disk. The obscuration of the central star was also obtained from the fit. S CrA is a close (one arcsecond) separation binary in which both components are pre-main sequence stars. Our observations reveal extended disk-like structures surrounding both components of the binary system. There also appears to be either a knot of material between the two stars or a faint third component in the system.

### Late-type Supergiants

Several new measurements of the position angle of the close companion to the supergiant  $\alpha$  Ori have been made. We have also discovered a large bright structure (or few unresolved structures) on the surface of  $\alpha$  Ori which are probably related to the phenomenon of stellar super-granulation.

We have detected an elongation of  $\alpha$  Ceti's (Mira) upper atmosphere (from observations obtained at two phases of the pulsation cycle of the star). This structure is probably associated with a disk around the star or a molecular cloud in the vicinity of the star formed as a result of stellar pulsations.

### REFERENCES

Ayers, G.R. and Dainty, J.C. (1988), "Iterative Blind Deconvolution Method and its Applications", Opt. Lett., 13, p.547.

Fienup, J.R. 1978, Opt. Lett., 3, 27.

Karovska, M., Nisenson, P., and Noyes, R. (1987), "High Angular Resolution Speckle Imaging of Alpha Ori", BAAS, Vol.19, No. 2.

Karovska, M., Koechlin, L., Nisenson, P., Papaliolios, C., and Standley, C. (1989), "Evidence for Asymmetries in SN1987A", to appear in *Highlights in Astronomy*, Vol. 8., ed. W. Liller, Kluwer Academic Publishers.

Karovska, M., Nisenson, P., Papaliolios, C., Stendley, C. (1989), "High Angular Speckle Observations of SN1987A. Days 40-580.", *BAAS*, Vol. 20, No. 4.

Karovska, M., Koechlin, L., Nisenson, P., Papaliolios C., Standley, C. (1989) "Measurements of the Diameter of the LMC Supernova SN1987A", *Ap. J.*, 340, 435.

Lane, R.G. and Bates, R.H.T. 1987, *J. Opt. Soc. Am. A*, 4, 180.

Moranais D. and Nisenson P. (1988), "Phase Reconstruction in Optical Interferometry", Proc. NOAO-ESO Conference on "High Resolution Imaging by Interferometry", 4 March, Garching, West Germany, p. 653.

Nisenson, P., Papaliolios, C., Karovska, M., and Noyes, R. (1987), "Detection of a Very Bright Source Close to the LMC Supernova SN1987A", *Ap. J. Letters*, 320, L15.

Nisenson, P., Karovska, M., Noyes, R., Papaliolios, C., Stachnik, K., Strom, S., and Edwards, S. (1987), "Speckle Imaging at CfA", *BAAS*, Vol. 19, No. 2.

Nisenson, P., Karovska, M., (1987), "Speckle Imaging at CfA", Proc. ESO-NOAO Conference on "High Angular Resolution in Astronomy", Jan. 5-8, Tucson, Az.

Nisenson, P., Karovska, M., Koechlin, L., Papaliolios, C. and Standley, C. (1988), "High Angular Resolution Imaging of SN1987A", Proc. NOAO-ESO Conference on "High Resolution Imaging by Interferometry", 14 March, Garching, West Germany, p. 491.

Nisenson, P. (1989), "Speckle Imaging with PAPA Detector and the Knox-Thompson Algorithm", Proceedings of the NATO Advanced Study Institute, Sept. 13-23, Cargese, France, Kluwer Academic Publishers.

Popham, R. (1988), "Speckle Observations of Young Stellar Objects", Senior Thesis,  
Harvard University.

Papaliolios, C., Karovska, M., Nisenson, P., and Standley, C. (1987), "SN 1987A and  
Companion", Fourth George Mason University Workshop in Astrophysics,  
"SN1987A in the LMC", eds. M. Kefatos, A.G. Michalitsianos.

Papaliolios, C., Karovska, M., Nisenson, P., and Standley, C. (1987), "SN 1987A and  
Companion", Fourth George Mason University Workshop in Astrophysics,  
"SN1987A in the LMC", eds. M. Kefatos, A.G. Michalitsianos.

Papaliolios, C., Karovska, M., Koechlin, L., Nisenson, P., Standley, C., and Heathcote,  
S. (1989), "Asymmetry of the Envelope of SN1987A, *Nature*, 338, 565.

Salas, I., Strom, S., Edwards, S., Stauffer, J., Nisenson, P., Karovska, M. (1989), "  
High Spatial Resolution Observations of Young Stellar Objects", *BAAS*, Vol.  
20, No. 4.

Standley, C., Karovska, M., Nisenson, P., Papaliolios, C. (1989), " Measurements of  
Stellar Angular Diameters Smaller than Telescope Diffraction Limit", *BAAS*, Vol.  
20, No. 4.

## APPENDICES

Appendix I: "Partial atmospheric correction with adaptive optics," Nisenson and Barakat, (1987), JOSA 4.

Appendix II: "Detection of a very bright source close to the LMC Supernova SN 1987A," (1987), Ap. J. 320.

Appendix III: "Asymmetry of the envelope of supernova 1987A," (1989), Nature 338.

Appendix IV: "Measurements of the diameter of the Large Magellanic Cloud Supernova SN 1987A," (1989), Ap. J. 340.

Appendix V: "Speckle imaging with the PAPA detector and the Knox-Thompson algorithm," to appear in Proc. NATO Advanced Study Inst., Cargese, France, Sept. 12-23, 1988 (Kluwer Academic Publ.)

# Partial atmospheric correction with adaptive optics

Peter Nisonson

Harvard-Smithsonian Center for Astrophysics, 60 Garden Street, Cambridge, Massachusetts 02138

Richard Barakat

Division of Applied Sciences, Harvard University, Cambridge, Massachusetts 02138

Received August 4, 1986; accepted August 18, 1987

Adaptive optics has seen only limited application in astronomical facilities, despite its significant potential for improving seeing conditions and increasing observing efficiency and productivity. Expense and technological difficulty appear to be the reasons that this is the case. Correction of large apertures requires hundreds of active elements in both the wave-front sensor and the adaptive mirror. We have performed some one-dimensional numerical simulations to test atmospheric wave-front correction when the active element is not matched to the correlation scale in the pupil. The results demonstrate that substantial seeing improvement can be obtained with an adaptive optical system having a limited number of active elements.

## 1. INTRODUCTION

The technology for the real-time correction of atmospheric aberrations using adaptive optics has been under development for more than a decade.<sup>1-4</sup> However, except for a few limited cases, these techniques have not been applied to optical astronomy, probably because of the difficulty and expense of the necessary technologies. Still, a technique that improves the atmospheric seeing would be of great benefit for almost all astronomical scientific programs, increasing magnitude limits, signal-to-noise ratio, and the observational efficiency.

Virtually all adaptive optical systems considered for seeing correction have been analyzed for the case when the scale of the active element (in the wave-front sensor and the adaptive mirror) matches the scale of the atmospheric correlation length ( $r_0$ ). For large telescopes, this means that, even for very good seeing (i.e.,  $<1$  arcsec), hundreds of correction elements are needed.<sup>5</sup> For example, 1-arcsec seeing with a 2-m telescope would require more than 400 active elements for diffraction-limited performance. When one combines this large number of active elements with the requirement for high-speed operation (1-msec cycle time), the adaptive optical system becomes prohibitively expensive. In addition, even an optimized system will have a magnitude limit that restricts its utility to bright sources and a limited class of scientific problems.

An alternative approach is to consider the effects of an adaptive optical system with active elements having a scale that is much larger than  $r_0$ , with the goal of obtaining partial improvement in the seeing. For many astronomical problems even a limited improvement in seeing would yield substantial gains, reducing data integration times and enhancing image quality. Since each active element is increased in area, many more photons are detected per element, improving the magnitude limit of the wave-front measurement proportionately. The longer scales in the atmosphere should also have longer time constants, so the system's cycle time

would increase, again improving the magnitude limit and reducing the technological requirements. Finally, correction of only the longer-scale atmospheric structure could also result in a wider isoplanatic field, increasing the probability of finding a sufficiently bright offset star for wave-front measurement, permitting correction and integration on faint or extended sources.

In this paper we describe some numerical experiments that we have performed to test the concept of partial correction. We have generated some simulated one-dimensional atmospheric wave fronts, applied correction factors to the wave fronts for various spatial scales, and then calculated transfer functions, point-spread functions (psf's), and images for intercomparison. The results support the thesis that substantial improvement in imaging capabilities could be obtained, even with limited adaptive atmospheric correction.

## 2. WAVE-FRONT GENERATION AND CORRECTION

The psf<sup>6</sup> for a slit aperture, without scintillation or deterministic aberrations, is

$$t(\nu) = \left| \frac{1}{2} \int_{-1}^{+1} \exp[ikZ(p)] \exp(i\nu p) dp \right|^2. \quad (2.1)$$

$Z(p)$  is the spatially random wave-front aberration function over the exit pupil induced by the turbulent atmosphere. We model  $Z(p)$  as a zero-mean, spatially stationary random process:

$$\langle Z(p) \rangle = 0, \quad (2.2)$$

$$\langle Z(p_1)Z(p_2) \rangle = \sigma^2 r(|p_2 - p_1|), \quad (2.3)$$

where  $\sigma^2$  is the variance of the random wave front measured in  $\lambda$  units and  $r(\Delta p)$  is the wave-front correlation function [the generation of sample realizations of  $Z(p)$  is outlined in

Appendix A]. The  $1/e$  width of  $r(\Delta p)$  is set to the approximate width of the Kolmogorov 5/3 power-law structure function,<sup>7</sup> the latter being the more conventionally chosen atmospheric mode.<sup>8</sup> We take

$$r(\Delta p) = \exp[-a^2(\Delta p)^2]. \quad (2.4)$$

where the parameter  $a$  governs the width of the wave-front correlation function relative to the aperture. This Gaussian correlation function was chosen for its analytical properties and computational simplicity.<sup>7</sup> A value of  $a = 1.3$  gives the approximate match to the Kolmogorov structure function.

Because the correlation function in Eq. (2.4) is so broad (when  $a = 1.3$ ), its Fourier transform is very narrow, and a large number of samples are needed if one is to avoid aliasing effects. To achieve the proper sampling, we insert the correlation function in a 2048-sample array; however, only the central 128 points of each wave front were used in the correction tests. For the numerical computations carried out in this paper, 128 sample realizations of  $Z(p)$  were generated (for fixed values of  $\sigma^2$  and  $a$ ).

PSFs  $t(\nu)$  and their corresponding spatial transfer functions

$$T(\alpha) = \int_{-\infty}^{+\infty} t(\nu) e^{-i\alpha\nu} d\nu \quad (2.5)$$

were evaluated, before and after wave-front correction, for each sample realization of the wave front that was generated.

Two correction algorithms were tested. In the first approach, each segment of the wave front was fitted with a straight line, using the first and last points of the segments to define the slopes of the line segments. This is a rather simplistic correction approach, mimicking an algorithm that might be used with a segmented adaptive mirror. In effect, it yields a worst-case result, since better fitting of the segments could be carried out with more-complex algorithms. The second approach was to perform a least-squares polynomial fit to the wave front with varying numbers of terms in the fit. This approach would be comparable to using a rubber mirror having a limited number of adaptive degrees of freedom. We found that when suitable parameters were chosen, the polynomial fitting gave similar results to the straight-line fit. However, the relationship between the fitting parameters and the physical characteristics of the mirror was far less obvious. Therefore in this paper we show only the results from the straight-line fit.

### 3. RESULTS

Figure 1 shows four of the simulated wave fronts generated for  $a = 1.3$  and  $(\sigma/\lambda) = 2.31$ , which give a corresponding value for  $(D/r_0) = 18.85$ .<sup>7</sup> In Fig. 2 we show examples of applying straight-line segment correction to wave front A for 0, 2, 4, 6, and 8 segments. It is clear that, even for a few segments, the phase excursions of the wave front are dramatically reduced. Figure 3(a) plots the uncorrected PSF obtained from wave front A. Figures 3(b), 3(c), 3(d), 3(e), and 3(f) show the PSFs obtained from wave front A after straight-line segment correction has been applied for 2, 4, 6, and 8 segment correction, respectively. Again, obvious improvement in the PSF is observed even for only two-segment correction (the overall PSF width is reduced), and the PSF becomes very narrow with increasing number of segments in the correction.

In order to test the effectiveness of the wave-front correction, we have calculated ensemble-averaged transfer functions for the 128 wave-front realizations before and after correction (Fig. 4). The transfer functions shown, after correction, are for 2, 4, 6, 8, and 16 straight-line segment correction. The 16-segment correction result is essentially identical to the diffraction-limited transfer function. We also have calculated the square modulus of the ensemble-averaged transfer function, corresponding to the transfer function that one would obtain for astronomical speckle interferometry (Fig. 5). As expected, the uncorrected transfer function shows the high-frequency enhancement expected in speckle interferometry. It is obvious from both sets of transfer functions that substantial gains are obtained, even when the correction-segment dimension is much longer than the atmospheric correlation length. In most cases even the high frequencies are enhanced, especially in the speckle transfer function.

The ensemble-averaged transfer functions were then used in a calculation of the image for a simple test object. An object consisting of three overlapping Gaussians, each hav-

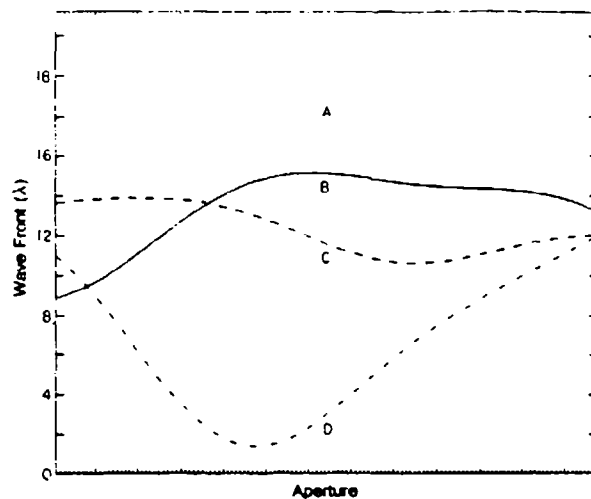


Fig. 1. Four sample realizations of  $Z(p)$  as measured in  $\lambda$  units from an ensemble having a correlation function of the form given by Eq. (2.4) with  $a = 1.3$  and  $\sigma = 2.31$ .

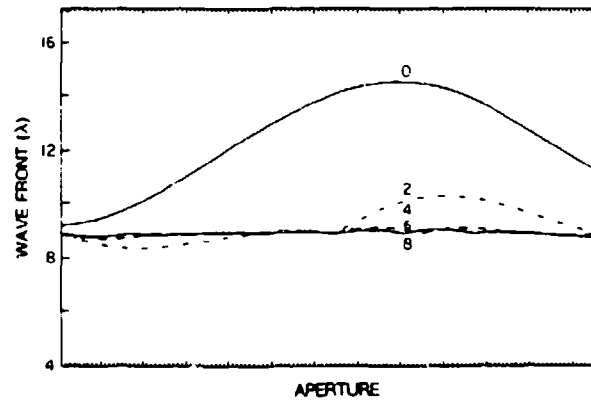


Fig. 2. Straight-line corrections of order 0, 2, 4, 6, and 8 applied to sample realization A of Fig. 1.

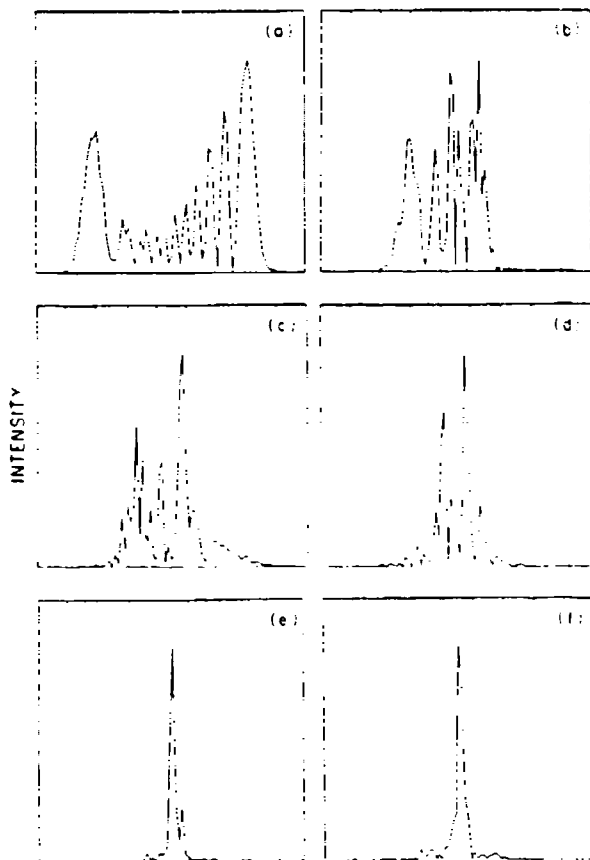


Fig. 3. PSFs derived for wave-front realization A in Fig. 1, with straight-line segment corrections: (a) no correction; (b), (c), (d), (e), (f) corrections of orders 2, 4, 6, 8, and 16, respectively.

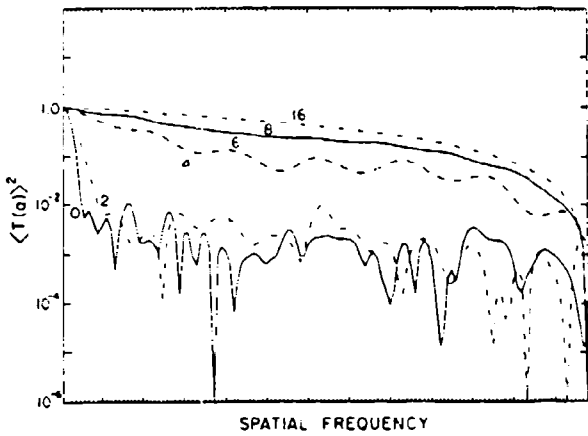


Fig. 4. Square ensemble average,  $\langle T(a) \rangle^2$ , for wave-front realization A in Fig. 1, with straight-line segment corrections of orders 0 to 16.

ing a different height and width, was chosen to represent an extended object of interest. The Fourier transform of the object was multiplied by various optical transfer functions and then retransformed to image space. Figure 6 shows the images for the cases of 0-, 4-, 8-, and 16-segment correction along with the diffraction-limited image.

The effectiveness of the correction was measured by calculating the mean-square difference between the diffraction-limited image and the uncorrected and partially corrected images. In Figs. 7(a) and 7(b) the results are plotted with logarithmic and linear ordinates, respectively. We have plotted both the result in which the average transfer function was used for the calculation and the result for wave front C, one of the least aberrated wave fronts in the ensemble. As would be expected from earlier results, these graphs show that the corrected images are converging to the unaberrated diffraction image, even for only a limited number of correction segments.

#### 4. DISCUSSION

The numerical experiments discussed in this paper demonstrate qualitatively that partial adaptive correction of the atmosphere can be an extremely useful technique for astronomical applications. However, the Gaussian model for the atmosphere is a substantial simplification and is certainly not accurate at all scales. In addition, the effects of scintillation, atmospheric scattering, and telescope aberrations have not been considered. Experimental verification of the results for a range of atmospheric conditions is essential

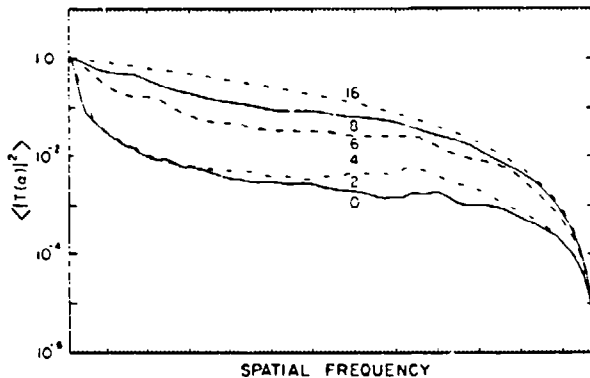


Fig. 5. Speckle transfer function,  $\langle |T(a)|^2 \rangle$ , for wave-front realization A in Fig. 1, with straight-line segment corrections of orders 0 to 16.

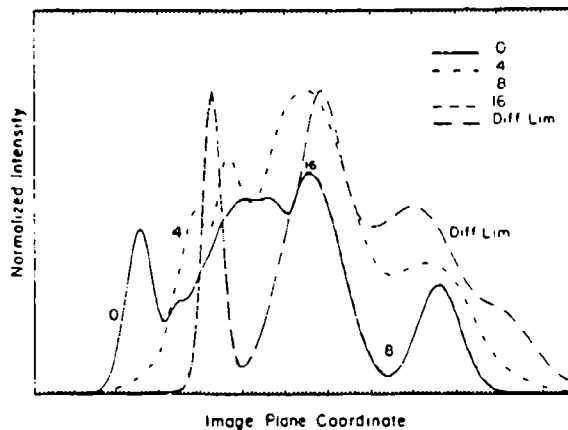


Fig. 6. Ensemble-averaged diffraction images of three-peaked Gaussian object corresponding to the corrected transfer functions shown in Fig. 4.

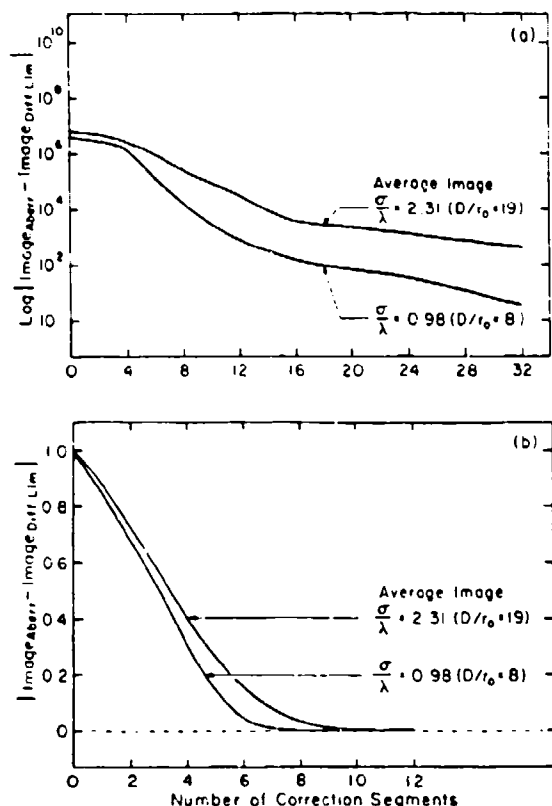


Fig. 7. Integrated modulus of differences between the diffraction-limited image of the three-peak Gaussian object and the corrected images shown in Fig. 6: (a) logarithmic display; (b) linear display.

before a large effort is put into implementing partial correction systems at astronomical sites. The range of applications to which the technique can be usefully applied is also highly dependent on the detailed atmospheric parameters. Questions that may be answered only by experimental measurement or a far more detailed analysis include the following: What is the degree of low-frequency spatial and temporal correlation? How large is the effective isoplanatic angle at low frequencies? What is the effect on the result of scintillation? ... of scattering? ... telescope aberrations? ... of errors in the wave-front sensing and correction? Answering these questions is beyond the scope of the current paper, requiring far more complicated modeling or experimental testing.

Despite these questions, there are many obvious astronomical applications for which partial adaptive correction could be of substantial benefit:

(1) Many spectroscopic sources are intrinsically faint and extended, requiring hours of integration time on large telescopes. Improvements in seeing would decrease the integration time proportionately, resulting in increased efficiency of large telescope time, a scarce and precious commodity. For many scientific problems, the improved spatial resolution could also be important. Of course, the success for faint-object spectroscopy will be critically dependent on being able to make wave-front measurements on off-axis

reference stars, which can be effective only if the low-angular-frequency isoplanatic angle is large.

(2) The search for protoplanetary material around bright stars (such as the discovery of a nebula around  $\beta$  Pictoris<sup>9</sup>) requires coronagraphic techniques as well as very low scattering, since the differences in brightness between the star and the nebula will be large. Implementation of partial correction before the coronagraph not only can permit more effective and closer-in blocking of the primary star but can also reduce the level of scattered light in the optics. Since the light from the star rejected by the coronagraph can be used for wave-front measurement, this should be an ideal application for correction, since no atmospheric assumptions are required for its success.

(3) Application of speckle imaging techniques after partial correction could permit near-real-time diffraction-limited image reconstruction. Since the number of frames required for convergence of the speckle process is proportional to the fourth power of the seeing, relatively small improvements in seeing could reduce the computation time required for reconstruction (without the use of supercomputers) sufficient to permit real-time data processing with conventionally available hardware.

It is clear that partial correction, leading to improved seeing, can have a significant effect on both efficiency and ground-based spatial resolution at many astronomical facilities, since improved seeing is almost equivalent to an increase in aperture size. Almost certainly, as the technology becomes available at an affordable level, many new applications will be recognized and implemented.

## APPENDIX A

We briefly outline the procedure used to generate sample realizations of the random wave front. We let

$$Z(p) = \sum_{m=-N}^N z_m \exp(i\theta_m) \exp[i(m\pi/L)p] \quad (A1)$$

in the fundamental interval  $|p| \leq L$ . The random variables  $\theta_m$  are uniformly distributed in  $|\theta_m| \leq \pi$  and are statistically independent. The  $z_m$  are as yet unspecified coefficients. Provided that  $N$  is large enough, then  $Z(p)$  is Gaussian distributed by virtue of the central-limit theorem.

We require that the mean of  $Z(p)$  vanish:

$$\langle Z(p) \rangle = \sum_{m=-N}^N z_m \langle \exp(i\theta_m) \rangle \exp[i(m\pi/L)p] = 0. \quad (A2)$$

The only way for this series to vanish is for

$$\langle \exp(\pm i\theta_m) \rangle = 0. \quad (A3)$$

This is true if the  $\theta_m$  are uniformly distributed over  $(-\pi, \pi)$ .

To evaluate the  $z_m$ , we form the covariance of  $Z(p)$ :  $\langle Z(p_1) Z^*(p_2) \rangle$ ; we can show that

$$\langle Z(p_1) Z^*(p_2) \rangle = \sum_{m=-N}^N z_m^2 \exp[i(\pi m/L)\beta], \quad (A4)$$

where  $\beta = |p_1 - p_2|$ . The  $z_m^2$  are given by

$$z_m^2 = \frac{1}{16} \int_{-2L}^{2L} \langle Z(p_1) Z^*(p_2) \rangle \\ \times \exp[i(\pi m/L)(p_1 - p_2)] d(p_1 - p_2). \quad (A5)$$

For the Gaussian wave-front covariance function, Eq. (2.4), this reduces to

$$z_m^2 = \frac{\sigma^2}{2L} \int_0^{2L} \exp(-\alpha^2 \beta^2) \cos\left(\frac{\pi m}{L} \beta\right) d\beta. \quad (A6)$$

These integrals were evaluated numerically. The series, (Eq. A1), was evaluated by the fast Fourier transform.

#### ACKNOWLEDGMENT

P. Nisenson wishes to thank Henry Radoski for his interest and support under grant AFOSR-86-0103 from the U.S. Air Force Office of Scientific Research.

#### REFERENCES

1. Special issue on adaptive optics, *J. Opt. Soc. Am.* 67(3) (1977).
2. J. W. Hardy, "Active optics: a new technology for the control of light," *Proc. IEEE* 66, 661-697 (1978).
3. J. Pearson, R. Freeman, and H. Reynolds, "Adaptive optical techniques for wavefront correction," in *Applied Optics and Optical Engineering*, R. Kingslake, ed. (Academic, New York, 1979), Vol. 7, pp. 245-340.
4. B. A. Horwitz and R. J. Becherer, eds., *Adaptive Optics Systems and Technologies*, Soc. Photo-Opt. Instrum. Eng. Proc. 365 (1983).
5. O. van der Lühe, "Adaptive image stabilization of solar observations: a review," in *High Resolution in Solar Physics*, R. Muller, ed. (Springer-Verlag, Berlin, 1985), pp. 62-82.
6. M. Born and E. Wolf, *Principles of Optics*, 4th ed. (Pergamon, Oxford, 1970), Chap. 9.
7. R. Barakat and P. Nisenson, "Influence of the wave-front correlation function and deterministic wave-front aberrations on the speckle image-reconstruction problem in the high light level regime," *J. Opt. Soc. Am.* 71, 1390-1402 (1981).
8. D. L. Fried, "Optical resolution through a randomly inhomogeneous medium for very long and very short exposures," *J. Opt. Soc. Am.* 56, 1372-1378 (1966).
9. R. J. Terrile and B. A. Smith, "A circumstellar disk around  $\beta$  Pictoris," *Science* 226, 1421-1424 (1984).

APPENDIX II

DETECTION OF A VERY BRIGHT SOURCE CLOSE TO THE LMC SUPERNOVA SN 1987A

P. NISENSON, C. PAPALIOLIOS, M. KAROVSKA, AND R. NOYES

Harvard-Smithsonian Center for Astrophysics

Received 1987 June 17, accepted 1987 June 30

ABSTRACT

High angular resolution observations of the supernova in the Large Magellanic Cloud, SN 1987A, have revealed a bright source separated from the SN by approximately 60 mas with a magnitude difference of 2.7 at 656 nm ( $\text{H}\alpha$ ). Speckle imaging techniques were applied to data recorded with the CfA two-dimensional photon counting detector (PAPA) on the CTIO 4 m telescope on March 25 and April 2 to allow measurements in  $\text{H}\alpha$  on both nights and at 533 nm and 450 nm on the second night. The nature of this object is as yet unknown, though it is almost certainly a phenomenon related to the SN.

*Subject headings:* interferometry — stars: supernovae

I. INTRODUCTION

The supernova SN 1987A in the Large Magellanic Cloud (LMC) is the closest unobscured event of its kind since 1604. This provides a unique opportunity for a detailed study of this extraordinary event using a wide variety of observational tools. At the 50 kpc distance of the LMC, high angular resolution interferometric techniques are capable of providing substantial information about the expanding shell and the environment around the SN.

On 1987 March 25 (30 days after the initial event) and on April 2, observations of the SN were made using the Cerro Tololo InterAmerican Observatory (CTIO) 4 m telescope and the Harvard-Smithsonian Center for Astrophysics (CfA) speckle imaging system. The planned purpose of the observations was to attempt to measure the angular diameter of the SN photosphere and to detect the relative position of the SN with respect to the Sanduleak B3 supergiant. At the time of these observations, it was uncertain whether this star still existed, though subsequent analysis of *JUE* spectral data has since shown (Kirshner *et al.* 1987) that the star probably cannot still be in its original form. Speckle observations could also be used to examine the region around the SN for possible light echos from surrounding dust or gas. Despite its expected angular size of only a few milliarcseconds (mas), measurement of the photospheric diameter appeared to be possible using aperture mask interferometry, since the high brightness of the source would provide very high signal-to-noise data. Details of this experiment will be included in a separate paper.

Conventional speckle data were recorded using the PAPA two-dimensional photon counting detector and a set of narrow band (10 nm half-power width) interference filters. Reduction of the data recorded at 656 nm ( $\text{H}\alpha$ ) from both nights produced a totally unexpected result, showing a bright source only 2.7 mag fainter than the primary source, and separated from it by approximately 60 mas (Karovska *et al.* 1987). A nearly identical result was obtained from the  $\text{H}\alpha$  data from the observations on both nights and the source was

also detected at 533 nm and 450 nm on the second night. This second object cannot possibly be the original Sanduleak star since it is about 6 mag brighter.

In this Letter, we will describe in more detail the observations and results, suggest possible interpretations, and discuss the follow-up observations needed to attempt to understand the mysterious nature of this second source.

II. OBSERVATIONS AND PROCESSING

Two nights, 1987 March 25 and April 2, were provided by the director of CTIO, Dr. R. Williams, for speckle observations of the SN. The speckle system used for these observations was constructed at CfA and has been described in detail elsewhere (Karovska, Nisenson, and Stachnik 1986). An important component of this system is the detector, the Precision Analog Photon Address detector (PAPA) (Papaliolios, Nisenson, and Ebstein 1985) which determines the x-y position and time of arrival of each detected photon. This detector has been shown to have the characteristics necessary for accurate speckle image reconstruction. The digital photon addresses are converted to a video signal and stored on VCR tape for later processing. The front-end optics package includes magnifying optics to match the telescope and detector resel scales, computer-controlled atmospheric dispersion correcting prisms, a set of narrow-band interference filters, and various neutral density filters.

The observations consisted of recording data sets of 5 minutes duration on the SN and three different reference stars. Data were recorded with four different filters centered on 400, 450, 533, and 656 nm, each with a bandwidth of 10 nm. Count rates for the data sets ranged from 40 to 70 thousand detected photons per second (neutral density filters were required to reduce the source brightness). The field size used for recording was 1.9" with 256 × 256 pixel sampling. This gives a 7 mas per resel which is more than adequate for sampling the diffraction limit of the 4 m telescope, which ranges from 20 mas at 400 nm to 33 mas at 656 nm. Since the

observations were made when the telescope was pointed between  $20^\circ$  and  $30^\circ$  from the horizon, the data were not of the best quality. Seeing was approximately  $2''$ , the atmospheric dispersion was not fully corrected at shorter wavelengths, and the telescope tracking was unsteady.

The first step in the data processing is flat-fielding, which corrects for nonuniformities in the photocathode and the camera. The photons are grouped into frames and then Fourier-transformed (FT). The optimum frame time was determined by integrating short sets of data with several different frame times and measuring the variance in the high frequency region of the FT. The frame time for the SN data turned out to be 5 ms. Approximately 60,000 frames were available for each data set. Complex correlations are calculated from the FT of each frame (Knox and Thompson 1974) to average both the amplitude and phase in the FT; these correlations are then summed over all the frames. Similar operations are applied to the reference star data, and division of the SN data by the reference star data in Fourier space performs an operation equivalent to deconvolution, eliminating the effects of the atmospheric transfer function and telescope aberrations. The inverse FT of the complex spectrum results in the reconstruction of an image. The transform of the squared modulus reconstructs an autocorrelation image (AC); the AC generally has better signal-to-noise ratio and is used for determining the magnitude difference of the two components. In the case of a simple object such as a binary star, the image is needed only to eliminate the  $180^\circ$  ambiguity in the position of the second component.

### III. RESULTS

Figure 1 (Plate L1) shows the results from the data processing. Figure 1a is a single input frame, showing the position of each detected photon in a single input frame. Flat fields were recorded by pointing the telescope at an illuminated screen on the dome, and the amplitudes in each frame were scaled by the integrated flat field, thereby correcting for system and detector nonuniformities. Figure 1b displays the power spectrum from the integrated transform of the 656 nm data recorded on April 2. Despite the noise in the display, one can see broad, low-contrast bands, which are the fringes characteristic of a close double star with unequal magnitude components. Figure 1c shows the image of an unresolved reference star, and Figure 1d shows the SN reconstructed image. The size of the displayed spots is indicative only of their relative brightness.

Data for nearby comparison stars recorded close in time through the same filters produced clean, pointlike images, with no significant structure at the separation and position angle of the second source in the SN images. Figure 2a plots the  $\text{H}\alpha$  AC, and Figure 2b shows the AC at 533 nm. These two ACs were generated using the central  $128 \times 128$  pixels in the field (7 mas sampling,  $0''.95$  field) which gives a somewhat better definition of the reconstructed peaks. Figure 2c shows the AC at 450 nm, reconstructed by averaging the finest pixels to produce a  $1''.9$  ( $128 \times 128$ ) field with 14 mas sampling. Figure 2d plots the reference star  $\nu$  Doradus which was recorded with the 450 nm data, also reconstructed at the larger scale. The averaging generally gives better signal-to-

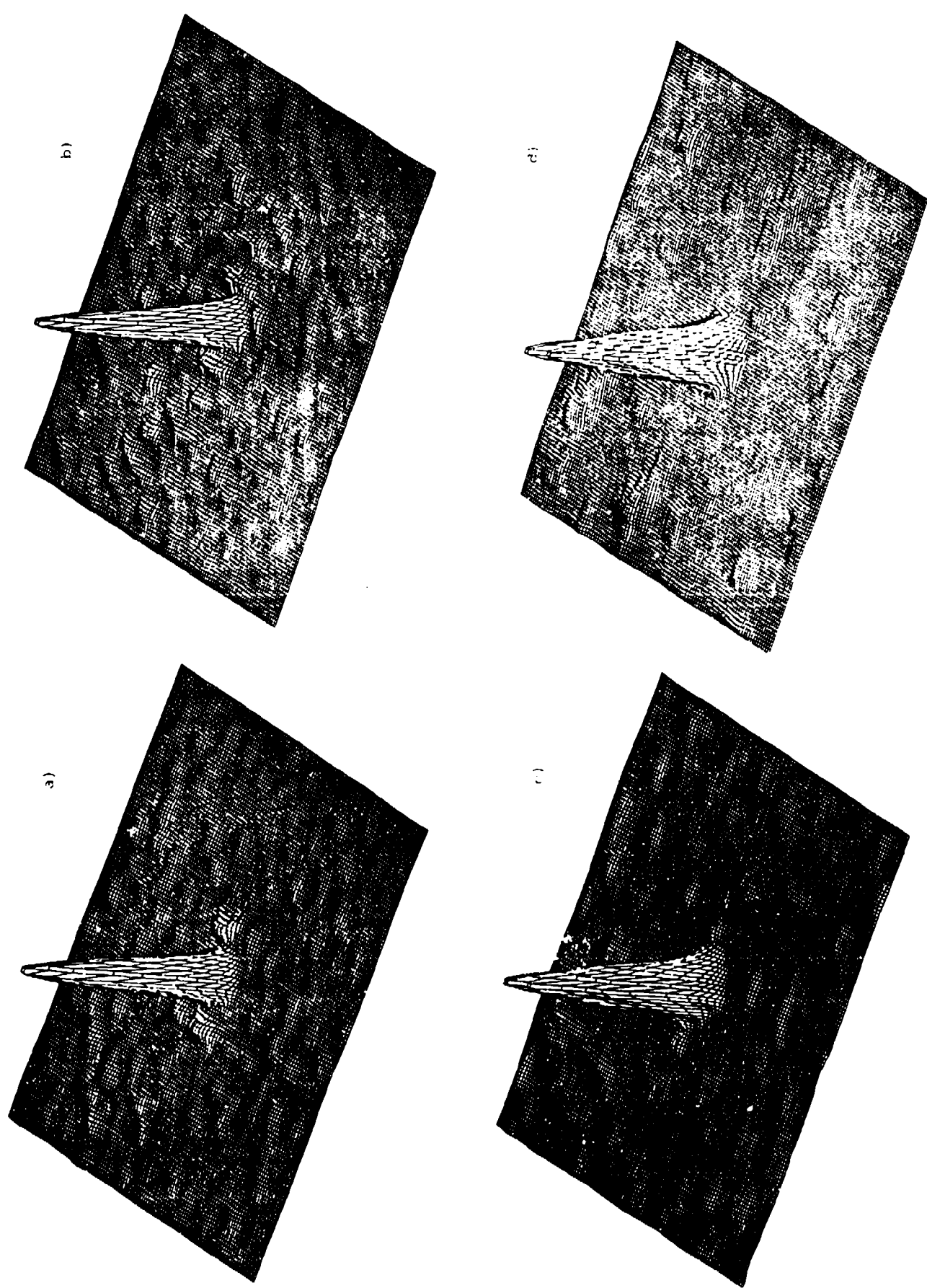
noise ratio, needed for the 450 nm reconstruction, but may result in an image which is slightly less sharp. It is clear that the double structure in the SN is well above the background noise level, particularly in  $\text{H}\alpha$ , and the reference star AC has no substantive structure at a comparable scale and position. The ACs, which are reconstructed from only the amplitudes in the transform, have better signal-to-noise ratio than the image, because of the more severe requirements on the quality of the data for the image reconstruction process. Therefore, they were used to measure the parameters of the reconstructed sources.

The separation of the two sources measured in  $\text{H}\alpha$  on both nights was  $0''.059 \pm 0''.008$ , and the magnitude difference was  $2.7 \pm 0.2$ . Since the visual magnitude of the SN at the time of the observations ranged from 4.0 (March 25) to 3.8 (April 2), this source has an apparent magnitude of about 6.5. The errors in our magnitude estimates are slightly too large (0.2) to allow a determination whether the second source changed in brightness by the same amount as the SN during the eight days between our observations. The measurement at 533 nm (April 2) gave a separation of  $0''.052 \pm 0''.007$ , and the measured magnitude difference was  $3.0 \pm 0.5$ . In both the  $\text{H}\alpha$  and 533 nm measurements, the position angle of the secondary source relative to the primary was  $194^\circ \pm 2^\circ$ . The  $180^\circ$  ambiguity normally associated with speckle interferometry measurements was eliminated using the image reconstruction. Reconstructions from data recorded at 450 nm show a feature at approximately the same position with a 3.5–4.0 mag difference from the primary. Residual atmospheric dispersion produced elongation in the reconstructions, and this was an increasingly severe problem at shorter wavelengths. Thus either residual dispersion or the red color of the source might explain the uncertainty of its detection at 450 nm. The elongation appears to be somewhat greater in the SN images than in the comparable reference stars, despite their having been close in position on the sky. This suggests that the elongation may be in the object, though the signal-to-noise ratio in the detection is too low to be sure.

### IV. DISCUSSION

The detection of the second bright source on two different nights, 8 days apart, combined with the reported detection of this source by a group at Imperial College performing speckle observations on the Anglo-Australian Telescope (Matcher, Meikle, and Morgan 1987) on April 14, leaves little doubt that the source really exists. Since this second source was almost 5 mag brighter than any known preexisting source in the field (the B3 Sanduleak star), it is clear that its appearance must be related to the SN. Reconstructions from the data recorded at 400 nm, where the SN was reduced sufficiently in brightness so that the magnitude difference between the SN and the B3 star would have been small enough to detect their separation, showed no extension of the primary source to an accuracy of about 20 mas. The 60 mas separation of the two bright sources would correspond to about 3000 AU at the distance of the LMC (50 kpc), perpendicular to the line of sight. This corresponds to 2 lt-weeks, and the first observation occurred 30 days after the SN explosion.

FIG. 2.—Speckle autocorrelation images of the region around SN 1987A in three wavelengths and a comparison star. (a) Autocorrelation in H $\alpha$ . (b) Autocorrelation at 511 nm. (c) Autocorrelation at 450 nm. (d) Autocorrelation of the reference star r Doradus at 450 nm.



One possible explanation for the existence of the second source is that it could be a large cloud of dust or gas reflecting light from the SN. However, the brightness of the second source would require that the cloud subtend a minimum of 1 sr as seen from the SN (the source is 10% as bright as the SN), even with an albedo of unity. This would be an enormous cloud, probably spatially resolved by our measurements. It is also unlikely that such a cloud could exist in the neighborhood of a B3 supergiant. Another possibility is that the second source was a very bright star wrapped in a dust shell which was blown away by the SN flash. However, such a source would be nearly the brightest star in the LMC (improbable) and would have been very bright in the IR. No such source existed in that position in the *IRAS* survey of infrared sources.

While there are many other more exotic possibilities to explain these results, it is clear that more data are needed to sort them out. Measurement at a later date should determine whether their relative positions have remained stationary and whether the second source has brightened along with the SN.

- Karovska, M., Nisenson, P., Noyes, R., and Papaliolios, C. 1987, *IAU Circ.*, 4382  
 Karovska, M., Nisenson, P., and Siachnik, R. V. 1986, *AJ*, 92, 4  
 Kirshner, R. P., Sonneborn, G., Crenshaw, D. M., and Nassiopoulos, G. E. 1987, *Ap J.*, 320, 602

M. KAROVSKA, P. NISENSEN, R. NOYES, and C. PAPALIOLIOS: Harvard-Smithsonian Center for Astrophysics, 60 Garden Street, Cambridge, MA 02138

Measurement at other wavelengths should determine what the relative color of the two sources is, and whether the second source is an emission-line object. New observations are planned at the end of 1987 May and in early July. It is hoped that they will shed new light on this extraordinary object.

We are deeply grateful to R. Williams for providing the 4 m observing time on such short notice, and to Oscar Saa and the entire crew at CTIO for their gracious, friendly, and invaluable assistance in getting the experiment running. We also wish to thank N. Carleton and S. Ebstein for their aid in our frantic last-second preparations of the equipment; I. J. Shapiro for his rapid support of the expedition; and R. Kirshner, J. Raymond, L. Hartmann, and W. Traub for numerous useful discussions and advice. We are also grateful to Henry Radoski of AFOSR for his continued belief in and support of the speckle program at CfA. This work has been supported under grant AFOSR-86-0103, NASA grant NGL-22-007-228, and Smithsonian Institution Research Opportunities and Scholarly Studies Programs.

#### REFERENCES

- Knox, K. T., and Thompson, B. J. 1974, *Ap J. (Letters)*, 193, 145  
 Matcher, S. J., Meikle, W. P. S., and Morgan, B. L. 1987, *IAU Circ.*, 4391, errata 1987, *IAU Circ.*, 4394 and *IAU Circ.*, 4413  
 Papaliolios, C., Nisenson, P., and Ebstein, S. 1985, *Appl. Optics*, 24, 285

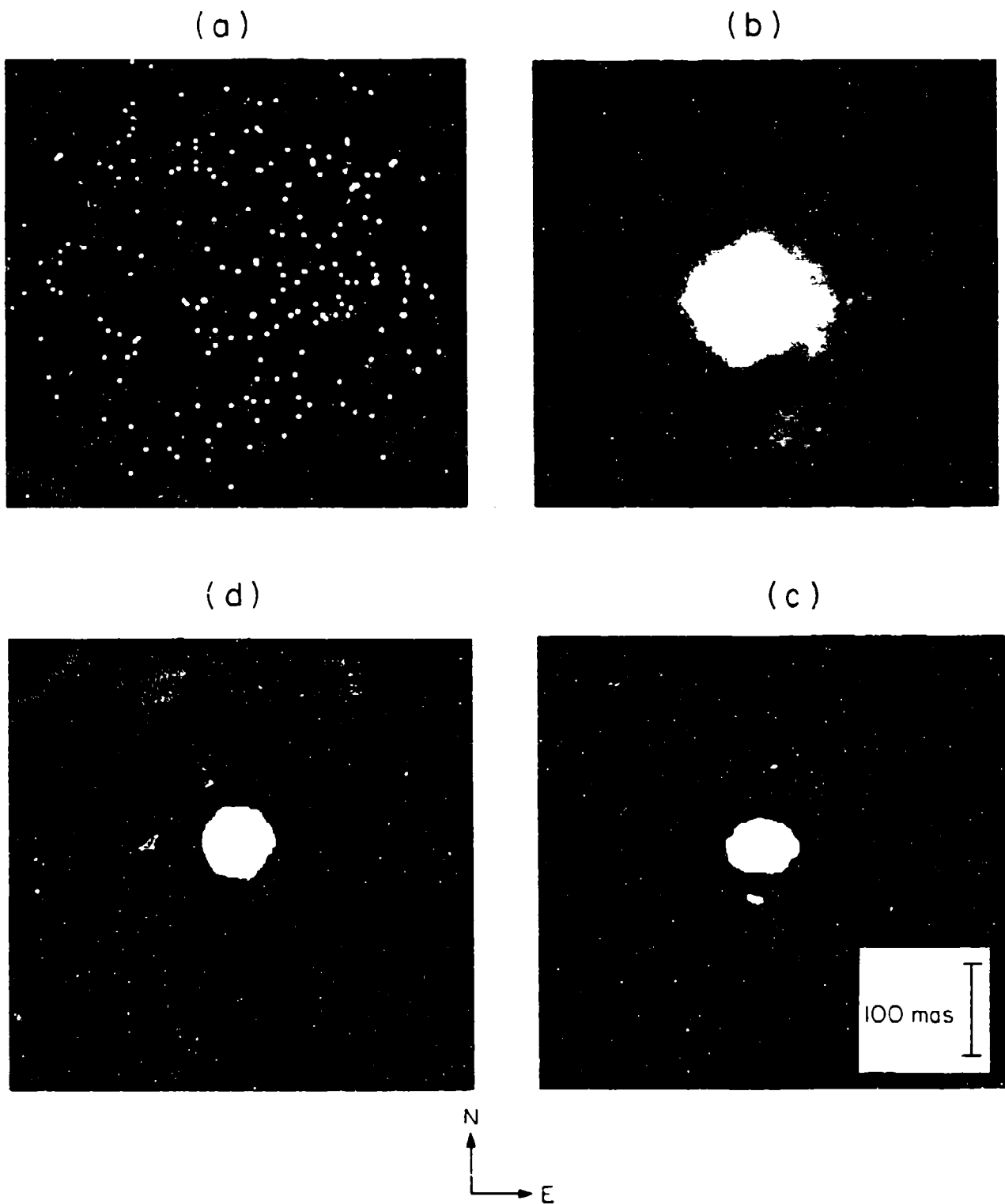


FIG. 1.—Speckle imaging reconstruction in H $\alpha$  of the region around SN 1987A showing the bright secondary source (a) Single 5 ms frame (b) reconstructed power spectrum from 60,000 frames. (c) Reconstructed image of the reference star  $\nu$  Doradus. (d) Reconstructed image of the SN NISENSON *et al.* (see 320, L16)

## Asymmetry of the envelope of supernova 1987A

C. Papaliolios\*, M. Karovska\*, L. Koechlin\*,  
 P. Nisenson\*, C. Standley\* & S. Heathcote†

\* Harvard-Smithsonian Center for Astrophysics, 60 Garden St, Cambridge,  
 Massachusetts 02138, USA  
 † Cerro Tololo Interamerican Observatory, La Serena, Chile

THE supernova SN1987A in the Large Magellanic Cloud has been observed by high-angular-resolution speckle interferometry since 25 March (30 days after the explosion) with the 4-m telescope at the Cerro Tololo Interamerican Observatory. These observations have provided a number of results that may be central to a detailed understanding of this unique event. Data obtained on 25 March and 2 April 1987 revealed a second bright 'companion' source separated from the supernova by 60 milliarcseconds and less than three magnitudes fainter than the supernova<sup>1</sup>. Measurements of the average diameter of the supernova envelope have been made from data recorded from March 1987 to April 1988<sup>2</sup>. Here we present a more detailed analysis of these data, which shows that the expanding envelope is asymmetric. This asymmetry has been observable since June 1987. The ratio between the minor and major axes of the envelope profile is about 2–3, and the position angle of the major axis is  $20^\circ \pm 5^\circ$ , consistent with results reported from polarization measurements. The major axis is aligned with the position angle of the companion to the supernova.

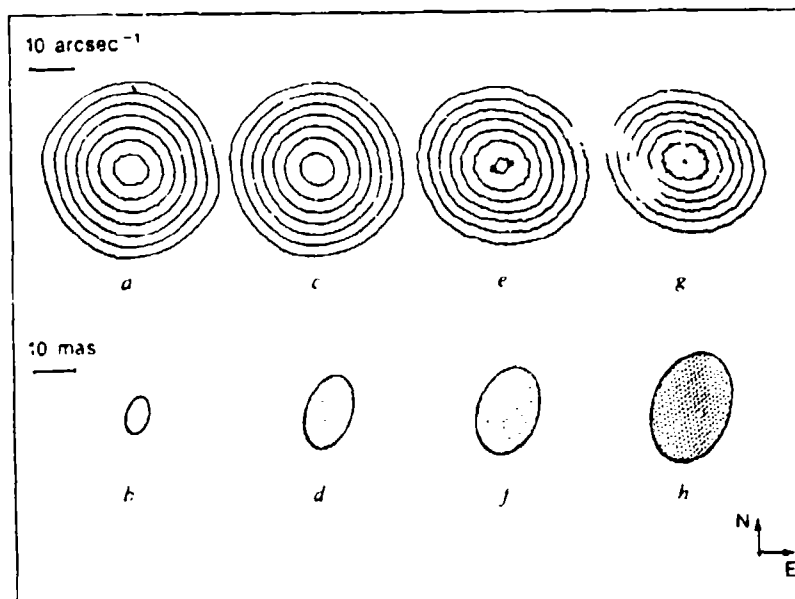
Speckle observations at optical wavelengths have been carried out using the PAPA detector<sup>3</sup>, a two-dimensional photon-counting sensor which records a catalogue of successive photon positions. The detector currently has a maximum data recording rate of 100,000 photon s<sup>-1</sup> in a field of 512 × 512 pixels. The speckle camera uses a fore-optics package which provides magnification of the image, so that the diffraction-limited scale of the telescope is matched to the pixel size of the camera, narrow-band optical filtering, which yields temporal coherence sufficient to allow interference over the path-length errors introduced by atmospheric aberrations, and atmospheric-dispersion correction, using a computer-controlled prism compensator. The digital output of the camera, in the form of photon addresses, is encoded on a video carrier and recorded with a VCR. The

stored addresses are recovered in the laboratory and unpacked for the speckle processing.

The photon addresses are grouped into frames, with a short time per frame relative to the atmospheric correlation time. This approach allows framing of the data for maximization of the signal-to-noise ratio in the integrated result; typical frame times range from 2 to 20 ms. Individual frames are built from the photon list by incrementing the number in the array position corresponding to the address of each detected photon. Corrections for the camera sensitivity (flat fielding) are made on the resulting frames. The Fourier transform for each frame is then calculated and accumulated into the power spectra and the complex correlation arrays which are required for diameter measurement and speckle image reconstruction using our version of the Knox-Thompson image-reconstruction algorithms<sup>4</sup>. Compensation for the atmospheric and telescope transfer function is accomplished by observing an unresolved comparison star immediately before and after the object observations. This star is chosen to be as close in angular position to the object as possible so that its atmospheric statistics are similar. Deconvolution by the reference star enhances the amplitudes of the high angular frequencies in the reconstruction. A detailed treatment of the algorithms and data processing is discussed elsewhere<sup>5</sup>.

Data sets on SN1987A and other stars result in diameter determinations with a precision of better than one milliarcsec. These measurements are made by fitting the integrated power spectra to the power spectrum of a uniform disk<sup>2</sup>, and, depending on the signal-to-noise ratio, can give results with resolution exceeding the diffraction limit of the telescope. Further analysis of the speckle data recorded between June 1987 (95 days after the explosion) and April 1988 (411 days after the explosion) shows that the expanding shell is elongated<sup>2</sup>. This asymmetry is detected from data recorded at several wavelengths between 442.0 nm and 850.0 nm. Figures 1a, c, e and g show the power spectra of SN1987A obtained from the data recorded near the centre of the H $\alpha$  emission line in May-June 1987, November 1987, February-March 1988 and April 1988. These powerspectra are elongated, with a major axis corresponding to a position angle (PA) in image space of  $20^\circ$  (or  $200^\circ$ )  $\pm 5^\circ$ . Similar departures from circular symmetry are seen in the power spectra obtained from data recorded in several different wavelengths. By fitting the power spectra of uniform-brightness ellipses to the observed power spectra, we determined the lengths of the

FIG 1 Speckle power spectra of SN1987A recorded in H $\alpha$  at four different epochs. (a, c, e, g) and ellipses showing schematically the size and orientation of the envelope at each epoch (b, d, f, h). a, b. June 1987. c, d. November 1987. e, f. February 1988. g, h. April 1988



major and minor axes, and their position angles. All of the measurements gave the same PA within the error bars. A summary of the measurements is given in Table 1. In contrast, data recorded on comparison stars give symmetric power spectra and symmetric images with measured angular diameters of less than 3 mas.

The ratio of the minor to major axis of the supernova's envelope is about 2-3 for all four data sets. The apparently increasing asymmetry in the supernova's power spectra shown in Fig. 1 is due to the increasing angular size of the supernova relative to the telescope's diffraction limit. Figures 1b, d, f and h show the ellipses whose Fourier transforms are fitted to the power spectra at the various epochs.

True images of SN1987A and its comparison star, ν Vol, were reconstructed using Knox-Thompson speckle-imaging techniques<sup>4</sup>. Figure 2 shows the images from data recorded in April 1988 at 533.0 nm (10-nm bandpass) and Hα (10-nm bandpass). The elongation of the supernova images, along an axis inclined at a position angle of 20° (or 200°), is quite evident despite the fact that its angular size in April was only slightly greater than the telescope's diffraction limit. Because the size of the image was so close to the telescope diffraction limit, the size of the axes were determined from power spectra, not from reconstructed images. The images also appear to be somewhat brighter in the south-west direction. The ν Vol images show no elongation and are symmetric. Their size is equivalent to the beam size for the reconstruction process.

In addition to our speckle results, other observations of SN1987A show strong evidence for an asymmetrically expanding shell<sup>6</sup>. Early spectroscopic observations (between 20 and 80 days after the explosion) detected a double-peaked feature in several hydrogen lines at optical and infrared wavelengths<sup>7-8</sup>. The appearance of two equally displaced components at longer and shorter wavelengths than the maximum emission was interpreted as being due to some departure from spherical symmetry of the shell.<sup>10</sup> Polarimetric observations<sup>11-14</sup> also show strong evidence for asymmetry in the envelope with a position angle of ~200°. The observed polarization structure was interpreted as arising from an asymmetrically expanding, scattering atmosphere. Polarimetric data were modelled by a scattering atmos-

TABLE 1 Measured asymmetries for SN1987A (PA = 200 ± 5°)

Days after explosion	$\lambda$ (nm)	Average diameter (mas)	Major axis (mas)	Minor axis (mas)
95-98 (May-June 87)	5.330	18 ± 2	19 ± 2	17 ± 2
	6.565 (Hα)	3 ± 1	10 ± 2	6 ± 2
	7.750	15 ± 2	20 ± 2	10 ± 2
265-268 (Nov. 87)	6.585 (Hα)	17 ± 1	18 ± 3	14 ± 3
	8.500	16 ± 1	20 ± 2	14 ± 2
	4.420	25 ± 2	27 ± 2	22 ± 2
	5.330	20 ± 1	24 ± 2	14 ± 2
	6.400	17 ± 1	20 ± 2	15 ± 2
370-373 (Feb.-Mar. 88)	6.565 (Hα)	21 ± 1	24 ± 2	16 ± 2
	7.000	17 ± 1	20 ± 2	16 ± 2
	8.500	18 ± 2	25 ± 2	12 ± 2
	5.330	26 ± 2	30 ± 2	20 ± 2
	6.565 (Hα)	27 ± 1	30 ± 2	20 ± 2
409-411 (April 88)	8.500	24 ± 2	28 ± 3	16 ± 3

sphere shaped as a prolate or oblate spheroid<sup>12,13,15</sup>. Best fits have been obtained for ratios of the smallest to the largest axis of these spheroids ranging from 0.6 to 0.9. Recently, γ-ray observations have yielded linewidths requiring either fragmentation or asymmetry of the supernova shell for their explanation<sup>16</sup>.

Present results from speckle interferometry, polarimetry, spectroscopy and γ-ray observations show that the expanding atmosphere of SN1987A is not spherically symmetric. The theoretical models that assume spherical symmetry must clearly be revised. An asymmetric envelope may also be necessary to explain, for example, the early emergence of X-rays and γ-rays and the evolution of their spectra with time<sup>17</sup>. Woosley<sup>18</sup> has suggested that non-uniformities in the collapse and core bounce could produce an asymmetric explosion, but that this asymmetry is far less likely to propagate to the outer envelope. Chevalier and Soker<sup>19</sup> have modelled the expanding supernova envelope and concluded that the most likely mechanism for asymmetry is rotational flattening of the progenitor envelope, probably requiring a binary companion during stellar evolution. Much of the evidence for asymmetries and extended structures around the supernova is summarized by Trimble<sup>20</sup>. □

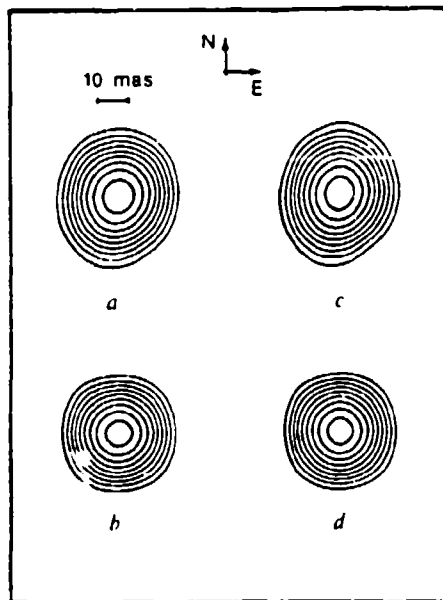


FIG. 2 Image reconstructions of SN1987A and a comparison star recorded in April 1988. a: SN1987A at 533.0 nm. b: Comparison star at 533.0 nm. c: SN1987A at Hα. d: Comparison star at Hα.

Received 23 January; accepted 24 February 1989

- Neanson, P., Papadopoulos, C., Karovitsa, M. & Hayes, R. *Astrophys. J.* **320**, L15-L18 (1987).
- Karovitsa, M., Koehlein, L., Neanson, P., Papadopoulos, C. & Standley, C. *Astrophys. J.* (in the press).
- Papadopoulos, C., Neanson, P. & Euston, S. *Appl Opt.* **24**, 287-292 (1985).
- Neanson, P. *Proc. NATO Adv. Study Inst. Cargese, France Sept.* 13-24 (Kluwer Amsterdam, in the press).
- Karovitsa, M., Koehlein, L., Neanson, P., Papadopoulos, C. & Standley, C. *IAU Circ.* No. 4804 (1988).
- Karovitsa, M., Koehlein, L., Neanson, P., Papadopoulos, C. & Standley, C. in *Highlights in Astronomy*, Vol. 8 (ed. Miller, W. C.) (Kluwer Amsterdam, in the press).
- Hauschke, R. W. & Debs, J. *Astr. Astrophys.* **182**, L29-L30 (1987).
- Philips, M. M. in *Proc. 4th George Mason University Workshop in Astrophysics: SN 1987A in the LMC* (eds Kafatos, M. & Michalakis, A. G.) 18-38 (Cambridge University Press, 1988).
- Denziger, I. J. et al. in *Proc. 4th George Mason University Workshop in Astrophysics: SN 1987A in the LMC* (eds Kafatos, M. & Michalakis, A. G.) 37-50 (Cambridge University Press, 1988).
- Lucy, L. B. in *Proc. 4th George Mason University Workshop in Astrophysics: SN 1987A in the LMC* (eds Kafatos, M. & Michalakis, A. G.) 323-334 (Cambridge University Press, 1988).
- Schwarz, H. E. & Mundt, R. *Astr. Astrophys.* **177**, L4 (1987).
- Mundt, M., Cicchetti, A., Benvenuto, O. G., Feinstein, C. & Marraco, H. G. *Astrophys. J.* **334**, 295-307 (1988).
- Chester, M. et al. *Mon. Not. R. Astr. Soc.* **233**, 695-722 (1988).
- Bailey, J. in *Elizabeth and Frederic White Research Conference on Supernova 1987A* (Proc. astr. Soc. Aust.) (in the press).
- Jeffery, D. T. *Nature* **328**, 419-421 (1987).
- Tsvetanov, B. J. et al. *Bull. Am. astr. Soc.* **20**, 1069 (1988).
- Gritsevich, S. A. & Sunyaev, R. A. *Soviet Astr. Lett.* **13**, 1042-1054 (1987).
- Woosley, S. E. in *IAU Symp. 125: The Origin and Evolution of Neutron Stars* (eds Helfand, D. J. & Huang, J.-M.) 255-272 (Reidel, Dordrecht, 1987).
- Chevalier, R. A. & Soker, N. *Astrophys. J.* (in the press).
- Trimble, V. *Rev. mod. Phys.* **60**, 859-871 (1988).

ACKNOWLEDGEMENTS We are grateful to R. Williams for granting us observing time on the CTIO 4-m telescope for this project and to the CTIO staff for their assistance. We thank R. Prochnow for his help with elliptical fitting routines. This work has been partially supported by the Smithsonian Institution Scholarly Studies and Research Opportunities grant programs. L.K. is Visiting Scientist from CERGA, Grasse, France.

## MEASUREMENTS OF THE DIAMETER OF THE LARGE MAGELLANIC CLOUD SUPERNOVA SN 1987A

M. KAROVSKA,<sup>1</sup> L. KOEHLIN, P. NISENSON, C. PAPALIOLIOS, AND C. STANLEY

Harvard-Smithsonian Center for Astrophysics

Received 1988 August 29; accepted 1988 September 30

### ABSTRACT

We present direct measurements of the angular diameter of SN 1987A in the Large Magellanic Cloud (LMC) made from high-angular resolution observations at the CTIO 4 m telescope in five observing runs from 1987 April to 1988 April. Diameters were determined to milliarcsecond precision from integrated power spectra, using speckle interferometric data. The accuracy of the technique was evaluated by laboratory experiments and measurements of the diameters of several stars of known angular size. The SN 1987A diameters measured near the center of the H $\alpha$  line show clear evolution during this period. The rate at which the supernova size changed at this wavelength corresponds to 2850 km s $^{-1}$  mean velocity of expansion. Diameter measurements obtained in several spectral lines and in the continuum indicate stratification of the expanding envelope of the supernova. Our continuum data yield diameters substantially larger than those calculated from photometric measurements and a blackbody fit to the observed spectra.

**Subject headings:** interferometry — stars: individual (SN 1987A)

### I. INTRODUCTION

High-angular resolution observations of SN 1987A provide valuable data that will contribute to the understanding of this extraordinary astrophysical event. Using speckle interferometric techniques, it is possible to overcome the resolution limits imposed by atmospheric turbulence and observe, in some detail, the morphology of the supernova (SN) and its environment. A wide variety of other observational techniques such as spectroscopy, photometry, and polarimetry are providing an extensive data base that, combined with the high-angular resolution measurements, will result in a detailed understanding of the mechanisms and dynamics of supernovae, thereby testing the validity of theoretical models.

Speckle observations at CTIO in 1987 March and April (Nisenson et al. 1987) have already revealed the presence of a second bright source 60 milliarcseconds (mas) from the SN and within a factor of 12 of its brightness. Observations at the AAT in 1987 April (Meikle, Matcher, and Morgan 1987), also using speckle techniques, produced supporting evidence for the second source. Furthermore, analysis of data acquired in five observing runs between 1987 April and 1988 April have provided measurements of the apparent diameter of the SN at several wavelengths. Diameter measurements were made by fitting the integrated power spectra obtained from the speckle process to the power spectrum of a uniform disk or a limb-darkened disk. Accurate fitting allows diameter estimates at scales well below the "diffraction limit" of the telescope, to a precision of a few milliarcseconds. Figure 1 illustrates the principle by which diameters well under the diffraction limit of the imaging system ( $\lambda/D$ , where  $\lambda$  is the wavelength and  $D$  is the telescope diameter) can be measured, showing the power spectra for stars with diameters 0.5, 1, and 2 times the diffraction limit. A star having an angular diameter smaller than the diffraction limit has a partial drop in power at the highest frequencies measured. Accurate measurement of this drop allows an estimation of the stellar diameter and this accuracy is only limited by the signal-to-noise ratio in the data. A recent

demonstration of this principle has been given by Davis and Tango (1986). Using a two-element interferometer with an 11 m baseline which has a resolution limit of 10 mas (at 550 nm), they were able to measure the diameter of Sirius (5.5 mas) to a precision of 0.08 mas. Similar results have been obtained using the I2T interferometer at CERGA (Koechlin and Rabbia 1985). While measurements of equivalent precision have not previously been demonstrated using speckle techniques, the validity of our results is supported by laboratory simulations and measurements of stars whose diameters have been determined by other methods.

### II. OBSERVATIONS AND PROCESSING

We report results from five observing runs using the Cerro Tololo Inter-American Observatory (CTIO) 4 m telescope. A summary of the observations is given in Table 1. Data were recorded using the PAPA two-dimensional photon counting detector (Papaliolios, Nisenson, and Ebstein 1986) and a front-end optics package. The optics package includes magnifying optics to match the telescope and detector pixel scales, atmospheric dispersion-correcting prisms, a set of narrow-band interference filters, and various neutral density filters. The camera records the x-y position and time of arrival of each photon event as it is detected, allowing construction of short-exposure speckle frames during the computer processing operations. A major advantage of this approach is that the optimum exposure time (as determined by the atmospheric correlation time) that maximizes the signal-to-noise ratio in the reconstruction may be determined during the data processing.

Data were recorded at many different wavelengths and under a variety of atmospheric conditions. The general approach was to record a relatively short data set (5 or 10 minutes) on the SN, preceded and followed by a 5 minute set on a comparison star. In all cases, the comparison stars were chosen to be single stars close in angular position to the SN and to have expected angular sizes as small as possible (less than 1 mas). The comparison stars were also chosen to be as bright as possible, yielding maximum signal-to-noise ratio in

<sup>1</sup> Visiting Scientist from CERGA, Avenue Copernic, 06130 Gresse, France

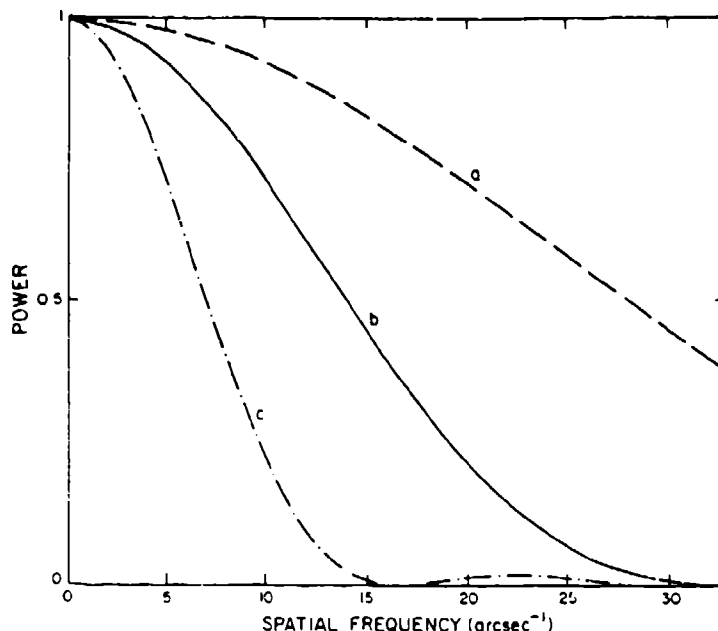


FIG. 1.—Ideal power spectra for stars with diameters (a) 0.5, (b) 1, and (c) 2 times the telescope diffraction limit. The right-hand axis corresponds to the 4 m diffraction limit at 6000 Å (33 arcsec<sup>-1</sup>).

the time allotted for their observation, since they are used in a deconvolution calculation during the data processing. The diameter of the detector field for all data sets was 1.95 with 256 × 256 sampling, giving a 7.5 mas pixel size. The SN and its comparison star were never higher than an altitude of 55°, and were as low as 20° for some of our observations, so they all required a large and accurate correction for atmospheric dispersion. Precise correction was performed using the pairs of computer-controlled Risley prisms in our optical front end.

TABLE I  
SUMMARY OF SPECKLE OBSERVATIONS

Date	Days after Explosion	Central Wavelength (nm)	Bandpass (FWHM) (nm)
1987 Apr 2 .....	38	450.2	10.0
		532.9	8.0
		656.5	10.7
1987 May 30-Jun 2 .....	95–98	450.0	10.0
		532.9	8.0
		656.5	10.7
		775.0	10.0
1987 Nov 15–18 .....	265–268	532.9	8.0
		640.0	10.0
		656.5	10.7
		658.5	10.0
		700.0	10.0
		850.0	25.0
1988 Feb 29–Mar 3 .....	370–373	442.0	32.8
		533.0	8.0
		640.0	10.0
		656.5	10.7
		700.0	10.0
		850.0	25.0
1988 Apr 8–10 .....	409–411	533.0	8.0
		656.5	10.7
		850.0	25.0

Since the comparison star's dispersion will be almost identical to that of the SN, any residual error due to dispersion will be corrected in the deconvolution during the data processing. The fit was only performed out to frequencies where both the reference and object power spectra were nonzero. The seeing was generally 2"-3" except in 1988 February, March, and April when seeing approached 1".

The first step in data processing is to calculate a flat field that corrects for the nonuniformities present in the photocathode sensitivity and the camera optics. The photons are grouped into speckle frames and each frame is flat-fielded before being Fourier transformed. The procedure for flat-fielding the data (Ebstein 1987) is to first generate a flat-field "mask" using a combination of "white-field" data (in which the camera is looking at the dome or an internal uniform source) and a filtered version of the long-exposure image of the object being flat-fielded. Use of the object data, itself, allows for any dynamic changes in the flat field and reduces the requirement of recording "white-field" data to about once per night. The synthesized flat field is then applied to each frame, after the photon addresses have been binned into individual frames. One ends up with frames in which each photon is given a fractional height proportional to the flat-field amplitude at that position.

The optimum frame time is determined by integrating the comparison star power spectra for several different frame times, calculating the variance and signal-to-noise ratio in the high-frequency region of the power spectrum and choosing the exposure time which maximizes the signal-to-noise ratio. Typical frame times were found to be about 10 ms, though they varied between 5 and 15 ms.

The ensemble average power spectrum is calculated for both the SN and its comparison star. Division of the SN power spectrum by the comparison star power spectrum corrects for the effects of the atmospheric and the telescope transfer functions. Diameter measurements were made by first azimuthally

averaging the power spectra to enhance the signal-to-noise ratio before division. A visibility function (the power spectrum of a limb-darkened or a uniform disk), in the form of the Hankel transform of the stellar profile was least-square-fitted to the ratioed power spectra with two free parameters, the width,  $a$ , and the amplitude,  $m$ . The diameter in image space was calculated from the width parameter,  $a$ . In the fitting procedure, the data were weighted by the autocorrelation of a circle. This corresponds to the fall off in signal-to-noise ratio with increasing spatial frequency of an ideal telescope with no atmosphere. Errors were estimated by calculating the standard deviations of the data from the fits. When the supernova power spectrum was divided by the corresponding comparison star power spectrum, the signal-to-noise ratio at the higher frequencies in both object and comparison star power spectra was low, so fitting was restricted to the low and intermediate frequency range. In addition, fluctuations in seeing between recording of the object and the comparison star make correction at the lowest few frequencies inaccurate. Despite these restrictions, this approach appears to give reproducible results, and application of this technique to stars with known diameter gives accurate results.

### III. LABORATORY SIMULATIONS

To check this technique, the same modeling and fitting was applied to data generated in laboratory simulations with disks of known diameter. The speckle camera system (including the PAPA detector) was set up to accept light from an optical system which simulates a telescope and a randomly varying atmosphere. The laboratory optics were scaled so that a 100  $\mu\text{m}$  pinhole placed 85 cm from the telescope aperture was just resolved at 656 nm. The diameter of the optical system pupil was adjusted so that the moving piece of ground glass used to

simulate atmospheric turbulence produced speckle images with the equivalent of 1"-2" seeing. The light level and spectral passbands were set to match the SN observation levels. Speckle data were recorded for three pinholes of diameters  $12 \pm 2$ ,  $50 \pm 5$ , and  $100 \pm 5 \mu\text{m}$ ; the 12  $\mu\text{m}$  pinhole was used as the comparison source after correction for its finite size by division of the appropriate Airy function. The power spectra and the best-fit Airy functions for the 50 and 100  $\mu\text{m}$  data are shown in Figure 2. The diameters calculated from the best fits to the data were  $55 \pm 3$  and  $100 \pm 3 \mu\text{m}$ . The accuracy of these results strongly supports the validity and precision of this technique for measuring diameters smaller than the diffraction limit of the imaging optical system.

### IV. RESULTS

In an important test of the performance of our technique, we measured the diameter of a solar-type star,  $\alpha$  Cen A. The data were recorded using the CTIO 4 m telescope on 1987 June 1 at 533.0 nm and 1988 February 29 at 450.0 nm. From both observing runs we obtained  $9 \pm 2$  mas for the angular diameter, assuming a uniform disk. Figure 3 shows the data from 1988 February and the corresponding best fit. When the effect of limb darkening is taken in account (Allen 1973, p. 120) the measured diameter of  $\alpha$  Cen A increases by approximately 10%. Our diameter measurement for  $\alpha$  Cen A is very close to the diameter of  $8.6 \pm 0.2$  mas obtained photometrically by Blackwell and Shallis (1977). The diameter of the red supergiant  $\alpha$  Sco at 533.0 and 656.5 nm was also measured. Figure 3 shows the data recorded in 1988 April (at 533.0 nm) using the CTIO 4 m telescope and the corresponding best fit. At the two wavelengths of observation we obtained  $35 \pm 1$  mas for the diameter of  $\alpha$  Sco, assuming uniform disk. When limb darkening is included, assuming a linear limb-darkening law, a dia-

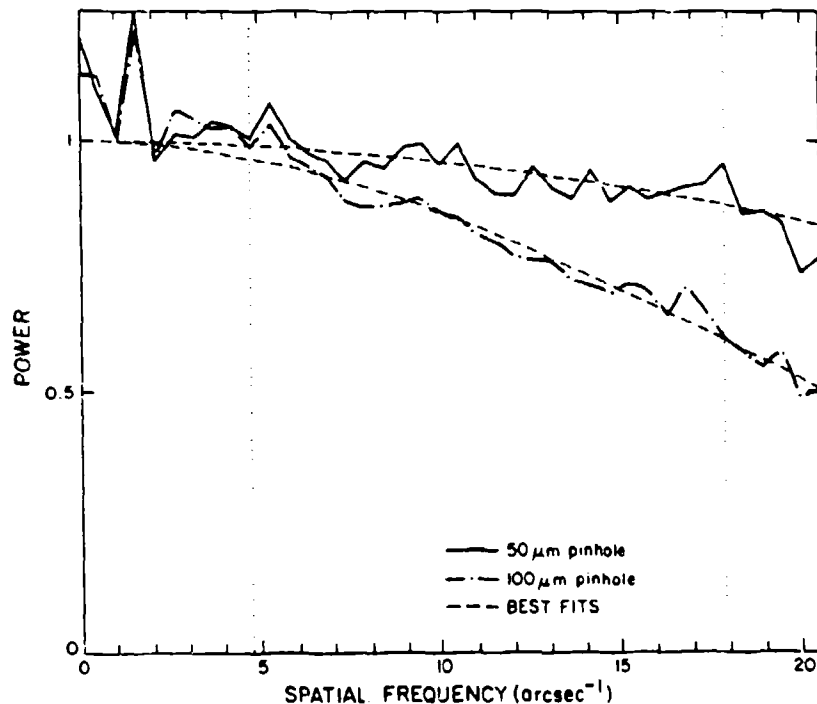


FIG. 2.—Laboratory simulation power spectra and best-fit Airy disks for the 50 and 100  $\mu\text{m}$  pinholes. Vertical dotted lines show the range of fitted region. The diffraction limit of the optical system at 656 Å was 30 arcsec $^{-1}$ .

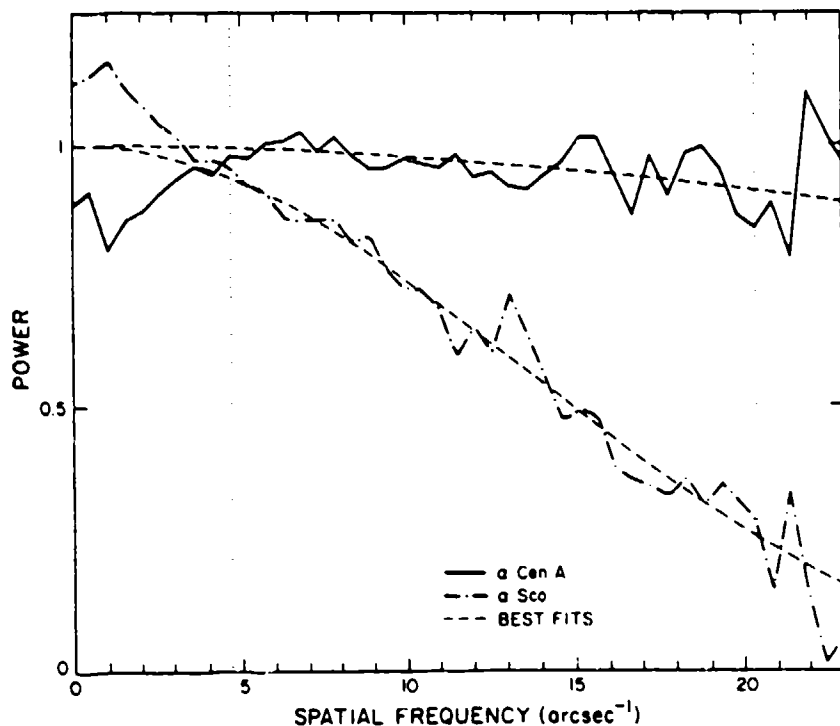


FIG. 3.—Power spectra for  $\alpha$  Cen A and  $\alpha$  Sco stars with known diameters. The best fits to the data (corresponding to a uniform disk of 9 mas for  $\alpha$  Cen A and 3.5 mas for  $\alpha$  Sco) are also plotted. Vertical dotted lines show the range of fitted region.

meter of  $39 \pm 1$  mas was obtained. These measurements are very close to the diameter of  $36 \pm 3$  mas, obtained by Blackwell and Shallis (1977). Also, they are in good agreement with the measurements from several observers using different techniques (summarized by White 1980).

Table 2 shows the summary of the results of diameter measurements of SN 1987A (assuming a uniform disk) made from data recorded at the five different epochs corresponding to the 38th, 95th–98th, 265th–268th, 370th–373d, and 409th–411th day after the explosion. While the data are not of sufficient quality to allow us to calculate the profile of the SN, the effect of limb darkening (or brightening) on the measured diameters can be estimated. Calculations show that extreme limb darkening (or brightening) will change the diameter measurement by no more than 15%.

From the March–April observations (at wavelengths of 450.0, 533.0, and 656.5 nm), the SN was found to be resolved at

450.0 nm (12 mas) and at 533.0 nm (11 mas), while at 656.5 nm it was essentially unresolved ( $\leq 5$  mas). The error bars for April measurements were relatively large ( $\pm 4$  mas) and reflect the relatively low signal-to-noise ratio in the power spectra due to poor seeing.

In May–June we measured the SN diameter at four wavelengths: 450.0, 533.0, 656.5, and 775.0 nm. The smallest diameter was measured at 656.5 nm ( $8 \pm 1$  mas). The diameters measured at 450.0, 533.0, and 775.0 nm were  $23 \pm 4$ ,  $18 \pm 2$ , and  $15 \pm 1$  mas, respectively.

In 1987 November diameter measurements were obtained at six different wavelengths: 530.0, 640.0, 656.6, 658.5, 700.0, and 850.0 nm. The diameters ranged from 15 mas at 640.0 nm to 20 mas at 533.0 nm. The signal-to-noise ratios in these data were higher than in the data from the two previous observing runs. This resulted in an improvement of the measurement accuracy (making it  $\pm 1$ –2 mas.)

We observed a substantial asymmetry in the data recorded in 1988 February–March and 1988 April at several wavelengths (Karovska et al. 1988). The images were elongated 30%–40% along an axis tilted  $20^\circ$ – $30^\circ$  from the north. Images of comparison stars and  $\alpha$  Cen A did not show this asymmetry. These results will be more extensively described in a separate paper.

In Table 2, we present our estimates of an “effective” diameter for the SN in 1988 February–March and 1988 April obtained by fitting the azimuthally averaged power spectra to visibility functions computed for different stellar disks with uniform brightness distribution.

Figures 4–6 show examples of the data and fitted curves. In Figure 4, we show the supernova in H $\alpha$  from the 1987 April run, an unresolved comparison star, and the fitted curves. The fit is a horizontal straight line for both of them, which is the expected result for an unresolved star. In Figure 5, we plot the

TABLE 2  
ANGULAR DIAMETER MEASUREMENTS OF SN 1987A\*

$\lambda$ (nm)	DAYS AFTER EXPLOSION				
	38	95–98	265–268	370–373	409–411
442.0	...	...	...	25 $\pm$ 2	...
450.0	12 $\pm$ 5	23 $\pm$ 4	...	...	...
532.9	11 $\pm$ 4	18 $\pm$ 2	20 $\pm$ 2	20 $\pm$ 1	26 $\pm$ 2
640.0	...	...	15 $\pm$ 1	17 $\pm$ 1	...
656.5	$\leq 5$	8 $\pm$ 1	18 $\pm$ 1	21 $\pm$ 1	27 $\pm$ 1
658.5	...	...	17 $\pm$ 1	...	...
700.0	...	...	17 $\pm$ 1	17 $\pm$ 1	...
775.0	...	15 $\pm$ 1	...	...	...
850.0	...	...	16 $\pm$ 1	18 $\pm$ 2	24 $\pm$ 2

\* Angular diameters are given in milliarcseconds. Errors correspond to  $1\sigma$ .

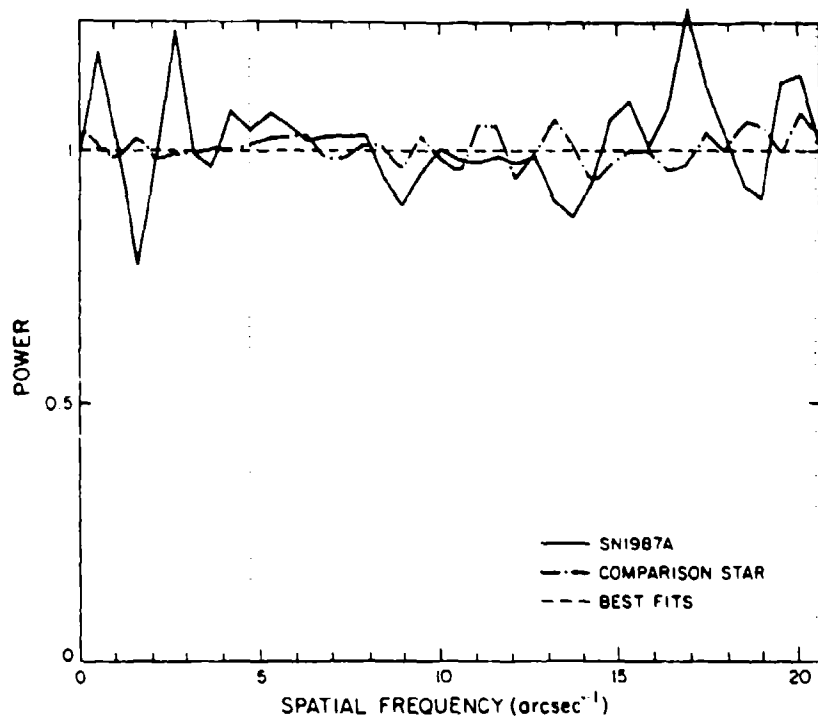


FIG. 4.—Power spectra and best fits for SN 1987A (1987 April) and an unresolved comparison star recorded in Hz. Vertical dotted lines show range of fitted region.

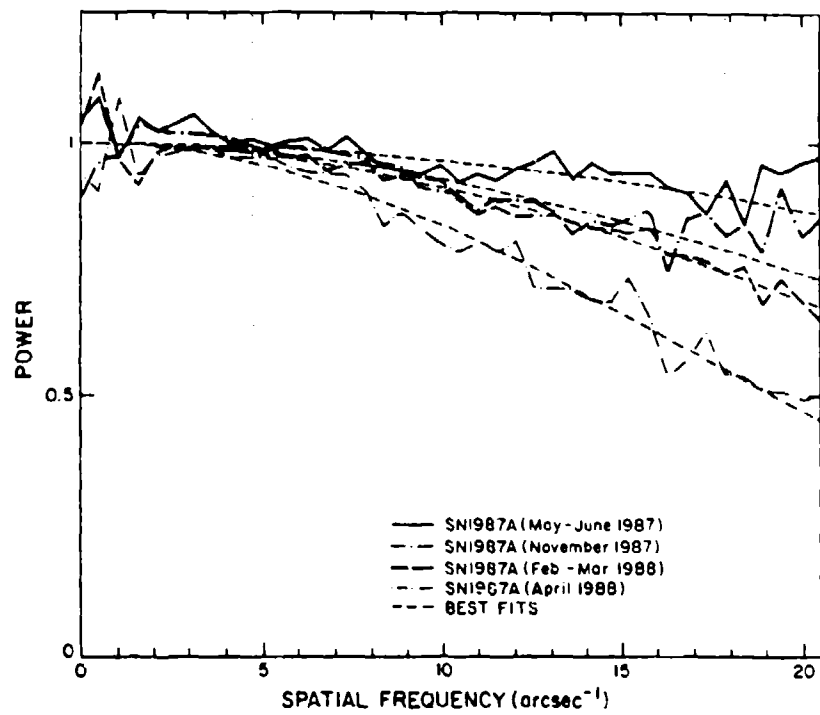


FIG. 5.—Power spectra and best fits for SN 1987A Hz data from 1987 May-June, 1987 November, 1988 February-March, and 1988 April observing runs. Vertical dotted lines show range of fitted region.

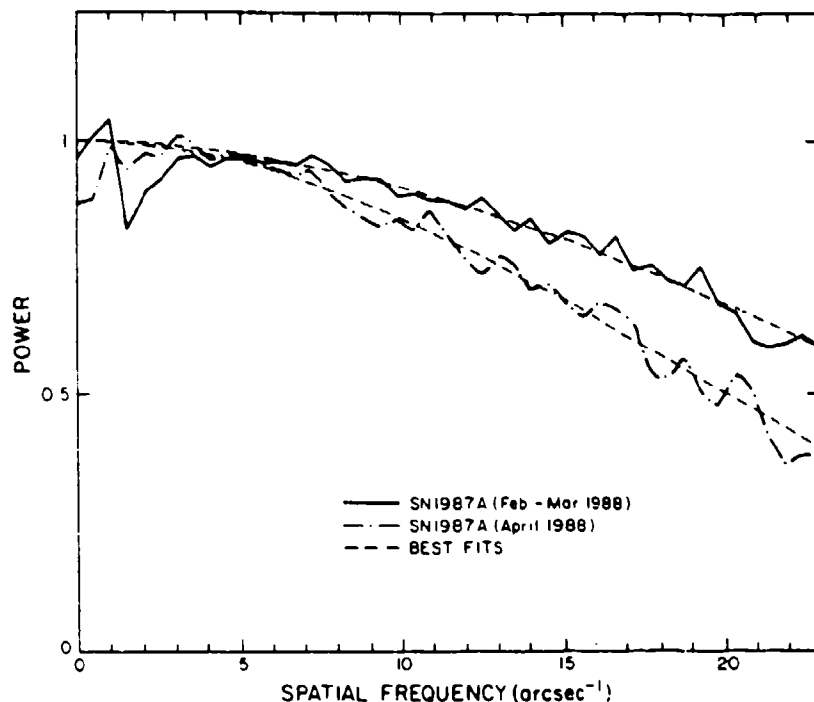


FIG. 6.—Power spectra for SN 1987A 533 nm data from 1988 February–March and April and corresponding best fits. Vertical lines show the range of fitted region

$H\alpha$  data from 1987 June, 1987 November, 1988 February–March, and 1988 April and their fits. The drop in high-frequency power between data sets corresponds to the increasing size in the SN diameter. In Figure 6, we show the 533 nm data and fits from 1988 February–March and 1988 April. The signal-to-noise ratio for these data was extremely good and allowed us to determine the SN diameter to an accuracy of better than 1 mas.

#### V. DISCUSSION

Our measurements of the SN diameter on April 2 (38 days after the explosion) and May–June (95–98 days after the explosion) show a substantial dependence on the wavelength of observation. At both epochs we obtained the smallest diameter at 656.5 nm and the largest at 450.0 and 533.0 nm. The 656.5 nm filter was located redward from the  $H\alpha$  absorption minimum and encompassed a large fraction of the P Cygni  $H\alpha$  emission feature (Phillips 1987). The 450.0 nm filter is in the absorption line corresponding to Ba II (Phillips 1987), while no prominent absorption or emission line could be distinguished in the 533 nm region. In May–June we observed the SN using an additional filter centered on the O I absorption feature at 775.0 nm. At this wavelength, the diameter is smaller than the one measured at 450.0 and 533.0 nm, but almost twice as large as the diameter measured at 656.5 nm.

The wavelength dependence of the measured diameters is probably due to the stratification of the expanding envelope of the SN. Evidence of stratification in the SN shell has already been found from spectral observations of the absorption minima of several spectral lines ( $H\alpha$ ,  $H\beta$ ,  $H\gamma$ , Ca II, Na I) during the first month of expansion (Hanuschik and Dachs 1987a, b). However, the fact that the angular diameter measured in the O I absorption trough is twice that measured in the  $H\alpha$  emis-

sion line requires that hydrogen lie within the oxygen shell, a result that is not predicted by current SN atmosphere models.

It is interesting to note, however, that the speckle diameters measured at the 656.5 nm spectral bandpass in 1987 April and May–June are consistent with the estimates of the effective diameters of the line-forming regions at both epochs. Figure 7

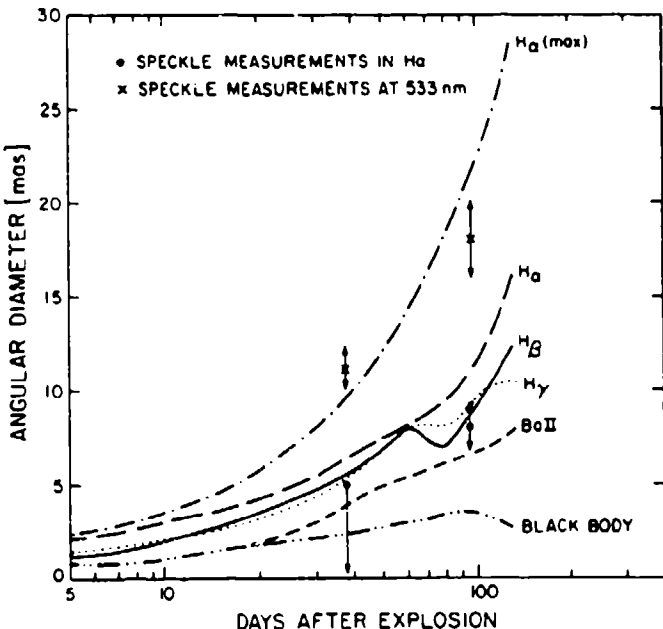


FIG. 7.—Diameters vs. time for SN 1987A calculated using velocities estimated from minima of various spectral lines and the blackbody photometric diameter estimates for the first 130 days since explosion (Phillips et al. 1988). The two measurements in  $H\alpha$  and at 533 nm are also shown.

shows the estimates of the effective diameters of the line-forming regions which were obtained by integrating the radial velocities corresponding to the absorption minima of several spectral lines during the first 130 days after the explosion (Hanuschik and Dachs 1987a, b; Phillips *et al.* 1988). On the 38th day after the explosion, the estimated angular diameter of the H $\alpha$  shell (i.e., the diameter of the region where H $\alpha$  becomes optically thick) is 6 mas, and we measured an angular diameter  $\leq 5$  mas at 656.5 nm. The angular diameter corresponding to the H $\beta$  and H $\gamma$  "shell" is around 5 mas. The estimated diameters derived from the radial velocity of the minimum of the Ba I absorption line is 2.8 mas. On the 98th day after the explosion we obtained an 8 mas diameter at 656.5 nm, which is in close agreement with the estimated effective diameter of 9 mas for the H $\beta$  and H $\gamma$  "shells," and a 7 mas diameter for the Ba II.

The diameters measured in the continuum bandpasses in 1987 April and 1987 May-June are substantially larger than those obtained from photometry and a simple blackbody fit to the observed spectrum (Catchpole *et al.* 1987; Danziger *et al.* 1987; Whitelock *et al.* 1988). These estimates of the SN diameter are shown in Figure 7. Larger continuum diameters obtained using speckle interferometry may be a result of electron scattering in the SN envelope. Lucy (1987) computed the "last-scattering" diameters (scaled to the blackbody photospheric diameter) for the 38th and 98th day after explosion. These computations were performed for the appropriate bandpasses of the speckle observations. Calculated diameters are 2-4 times larger than the blackbody diameter estimates, but they are still 1.5-3 times smaller than the diameters obtained using speckle interferometry. This suggests that the phenomenon of electron scattering cannot entirely account for the larger size of the SN measured by speckle interferometry. These models assume a uniform distribution of material in spherically symmetric shells. Clumpiness or asymmetries in the distribution of the material may well produce very different results.

The observations in 1987 November, 1988 February-March, and 1988 April were obtained during the period when the SN was already in its "nebular" phase. The SN diameter measured at 656.5 nm showed clear temporal evolution when compared with our earlier measurements at the same wavelength. Figure 8 shows the evolution of the H $\alpha$  diameter as measured by speckle interferometry during the first 411 days after the explosion. In addition to our measurements we show the speckle measurements near the center of the H $\alpha$  line obtained by Wood *et al.* (1988) on 1987 December 12 and 13, and 1988 February 20 using the Anglo-Australian Observatory 4 m telescope. The uniform disk angular diameters estimated for these two epochs are, respectively,  $23.1 \pm 1.6$  and  $23.9 \pm 0.9$  mas. We performed a linear least-squares fit to these data assuming that the diameter at the moment of the explosion was zero. If the increase of the diameter reflects the expansion of the SN atmosphere, then the slope of the fitted straight line gives a mean velocity of expansion of approximately  $2850 \text{ km s}^{-1}$ . Our measurement from February-March seems to underestimate the diameter of the SN at that epoch. This measurement has been affected by the asymmetry in those data.

Diameter measurements from the last three observing runs still show some dependence on the wavelength of observation, though the differences between the diameters measured in H $\alpha$  and in the other wavelengths are not as dramatic as they were in 1987 April and May-June. Diameter measurements in the 533 nm continuum from 1987 May-June and November and 1988 February are practically indistinguishable from one another. This is also true for the diameters measured at 640, 700, and 850 nm in 1987 November and 1988 February-March. If the 533 nm measurements correspond to the size of the SN photosphere then we conclude that they do not indicate any recession at these epochs.

At this point, it is difficult to find a simple interpretation for all our results. New, more detailed models for the SN are required. We plan to continue to monitor the changes in the SN diameter over a large spectral range and to follow the

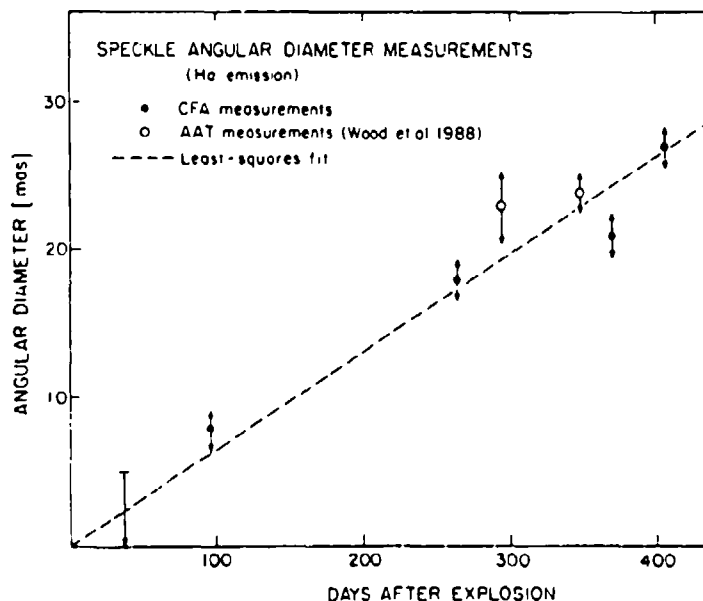


FIG. 8—Evolution of the SN diameter during the first 411 days after the explosion as observed by speckle interferometry techniques with  $3\sigma$  errors and best-fit straight line giving a velocity of  $2850 \text{ km s}^{-1}$ .

evolution of the expanding shell. If the present slow decline in brightness of the SN continues, we can observe the SN for several years before the magnitude limit of the speckle process is reached.

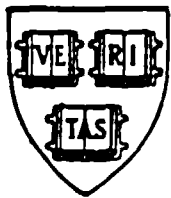
We are grateful to R. Williams for granting us observing time on the CTIO 4 m telescope for this project; to the CTIO staff for their invaluable assistance; to T. Varner for his help in the data reduction; to K. Hege and J. Christou for sharing

their November observing time with us; to R. Eastman, R. Kirshner, and R. Noyes for many helpful discussions; and to L. Lucy for his shared insights on supernova models. We are also grateful for the interest and support of I. I. Shapiro who aided us in obtaining travel support from Smithsonian Research Opportunities grant program and to H. Radoski of AFOSR who has provided continuing support for this project. This work has been partially supported under grant AFOSR-86-0103 and the Smithsonian Institution Scholarly Studies and Research Opportunities grant programs.

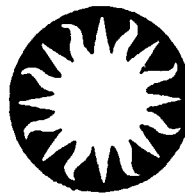
## REFERENCES

- Allen, C. W. 1973, *Astrophysical Quantities* (London: Athlone), p. 170.  
 Blackwell, D. E., and Shallis, M. J. 1977, *M.N.R.A.S.*, **180**, 177.  
 Catchpole, R. M., et al. 1987, *M.N.R.A.S.*, **229**, 15p.  
 Danziger, I. J., et al. 1987, in *Fourth George Mason University Workshop in Astrophysics, SN 1987A in the LMC*, ed M. Kafatos and A. G. Michalitsianos (Cambridge: Cambridge University Press), p. 37.  
 Davis, J., and Tango, W. J. 1986, *Nature*, **323**, 234.  
 Ebstein, S. M. 1987, Ph.D. thesis, Harvard University.  
 Hanuschik, R. W., and Dachs, J. 1987a, *Astr. Ap. (Letters)*, **177**, L4.  
 ——— 1987b, *Proc. ESO Workshop on SN 1987A*, ed. I. J. Danziger (Garching: ESO), p. 153.  
 Karovska, M., Koehlin, L., Nisenson, P., Papaliolios, C., and Standley, C. 1988, *IAC Circ. No. 4604*.  
 Koehlin, L., and Rahbja, Y. 1985, *Astr. Ap.*, **153**, 91.  
 Lucy, L. B. 1987, in *Fourth George Mason University Workshop in Astrophysics, SN 1987A in the LMC*, ed M. Kafatos and A. G. Michalitsianos (Cambridge: Cambridge University Press), p. 323.  
 Meikle, W. P. S., Matcher, S. J., and Morgan, B. L. 1987, *Nature*, **329**, 608.  
 Nisenson, P., Papaliolios, C., Karovska, M., and Noyes, R. 1987, *Ap. J. (Letters)*, **320**, L15.  
 Papaliolios, C., Nisenson, P., and Ebstein, S. 1985, *Appl. Optics*, **24**, 285.  
 Phillips, M. M. 1987, in *Fourth George Mason University Workshop in Astrophysics, SN 1987A in the LMC*, ed M. Kafatos and A. G. Michalitsianos (Cambridge: Cambridge University Press), p. 16.  
 Phillips, M. M., Heathcote, R., Hamuy, M., and Navarrete, M. 1988, *NOAO Preprint Series*, No. 144.  
 White, N. M. 1980, *Ap. J.*, **242**, 646.  
 Whitelock, P. A., et al. 1988, preprint.  
 Wood, P. R., Nulsen, P. E. J., Gillingham, P. R., Bessell, M. S., Dopita, M. A., and McCowage, C. 1988, preprint.

MARGARITA KAROVSKA, LAURENT KOEHLIN, PETER NISENSON, COSTAS PAPALIOLIOS, and CLIVE STANLEY: Harvard-Smithsonian Center for Astrophysics, 60 Garden Street, Cambridge, MA 02138



# Harvard-Smithsonian Center for Astrophysics



## Preprint Series

No. 2736

(Received October 7, 1988)

### SPECKLE IMAGING WITH THE PAPA DETECTOR AND THE KNOX- THOMPSON ALGORITHM

Peter Nisenson

Harvard-Smithsonian Center for Astrophysics

To appear in

Proceedings of the NATO Advanced Study Institute

Cargese, France

September 13-23, 1988

(Kluwer Academic Publishers)

HARVARD COLLEGE OBSERVATORY  
Sesquicentennial Year 1989

SMITHSONIAN ASTROPHYSICAL OBSERVATORY  
Centennial Year 1990

**Center for Astrophysics  
Preprint Series No. 2736**

**SPECKLE IMAGING WITH THE PAPA DETECTOR AND THE KNOX-  
THOMPSON ALGORITHM**

**Peter Nisenson  
Harvard-Smithsonian Center for Astrophysics**

# SPECKLE IMAGING WITH THE PAPA DETECTOR AND THE KNOX-THOMPSON ALGORITHM

PETER NISENSON

*Harvard-Smithsonian Center for Astrophysics*

*60 Garden St.*

*Cambridge, MA 02138*

*U.S.A.*

**ABSTRACT.** The speckle imaging program at the CfA has developed a set of tools for the implementation of speckle image reconstruction and has applied these tools to a wide range of scientific programs. Two key elements in this program have been the development of a 2-dimensional photon counting camera, the PAPA detector, and the implementation of image reconstruction procedures using the Knox-Thompson algorithm. This paper discusses the current status of the PAPA detector and the details of our data processing methods and numerical algorithms.

## 1. Introduction

Speckle interferometry is proving to be an invaluable tool for astronomical research, allowing measurements of a wide range of scientifically interesting objects that can be made in no other way. Most of the scientific results from speckle to date are in the areas of binary star orbits and stellar angular diameters. These objects are generally bright and have relatively simple geometries. Extending these techniques to a wider range of problems entails the observation of much fainter sources with, in many cases, more complex geometries. At the Center for Astrophysics (CfA), we have been concentrating on the development of detectors and algorithms that allow application of the speckle process to image reconstruction of faint, extended sources. The Knox-Thompson (K-T) algorithm (Knox, 1976) is one of a class of approaches to preserving the phase in the object Fourier transform, allowing true image reconstruction as an output of the process. The CfA application of the K-T algorithm has proven to be far more robust and accurate in its phase recovery process than Knox's original implementation due to several improvements in the technique. These improvements include the averaging of complex vector differences rather than phase differences and application of a least squares error distribution in the phase estimation process.

A crucial technology that allows the application of K-T to faint astronomical sources has been the development of the PAPA 2-dimensional photon counting camera. This detector records the spatial coordinates and time-of-arrival of each detected event, allowing the extremely accurate corrections for photon noise biases required for accurate reconstruction from the K-T process. The PAPA has proved to be a powerful and essential tool in the application of speckle imaging, providing the crucial linearity and dynamic range needed for accurate measurements of source characteristics. In this paper, the details of the CfA implementation of speckle imaging using the PAPA detector and modified versions of the K-T algorithm are discussed.

## 2. Data Recording

### 2.1 THE PAPA DETECTOR

The PAPA (Precision Analog Photon Address) detector (Papaliolios, et al, 1985) allows recording of the address (position) and time of arrival of each detected photon. A schematic diagram of the PAPA is shown in figure 1. The front end of the camera is a high gain image intensifier which produces a bright spot on its output phosphor for events detected by the photocathode. The back face (phosphor) of the intensifier is then reimaged by an optical system which is made up of a large collimating lens and an array of smaller lenses. Each of the small lenses produces a separate image of the phosphor on a binary mask. Behind each mask is a field lens which relays the pupil of the small lens onto a small photomultiplier (PMT).

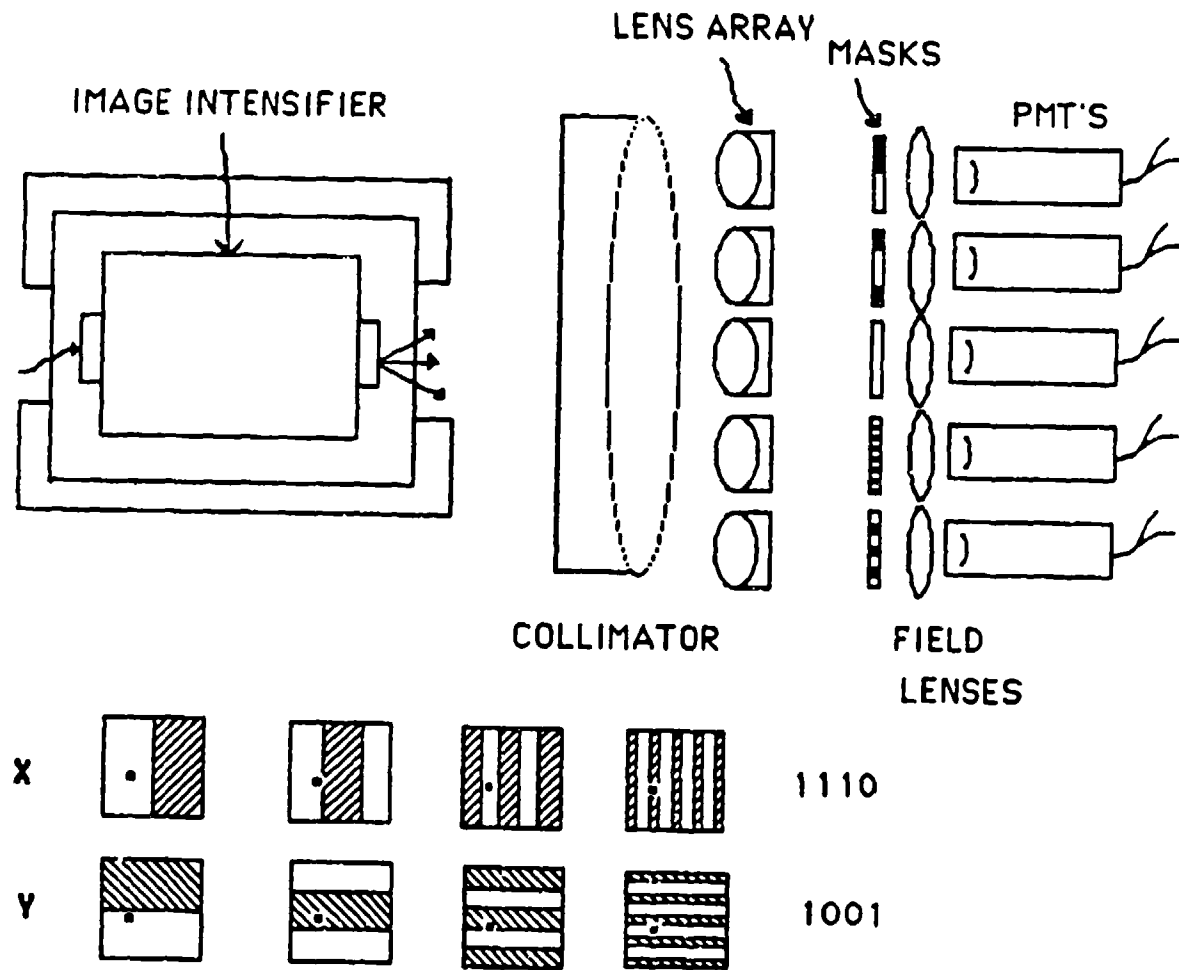


Figure 1. The PAPA Detector and Gray Scale Masks

The plan for the masks is shown at the bottom of figure 1. Each mask gives one bit of the digital address of the detected photon either in the x or y directions. One mask is completely clear, and this channel is called the strobe channel. When the strobe sees a pulse, signaling the detection of an event, the other channels are switched on and interrogated. A discriminator level is set for all the other channels, scaled to the height of the pulse detected by the strobe channel. If the photon image falls on the opaque part of the mask in a given channel, the output of the PMT will be below the discriminator level and that bit is set to zero. If the photon image falls on a clear area, the PMT sees a pulse above the threshold and the address bit is unity. The masks use a Gray (instead of binary) code which ensures that the mask stripes do not have edges located in the same place in the field.

The CfA PAPA has 19 channels giving 9 bit by 9 bit resolution (512x512) plus the strobe channel. We can currently record up to 100,000 event addresses per second from the camera. The inherent limit on the PAPA data rate is set by the decay time of the intensifier phosphor, (about 200 ns for P47), which suggests that the camera could operate at a rate over 1 million counts per second. The current camera uses only a single Gen II (channel plate) intensifier, which has only 3 to 4% quantum efficiency. New tubes which couple a Gen I diode in front of the Gen II have recently improved the peak quantum efficiency to over 10%. The high data rate requires special recording capabilities. At CfA, we have built a VCR digital recording system which encodes the digital output of the camera onto a video carrier, allowing the storage of two hours of telescope data on a single VHS tape (Ebstein, 1986). The data must be stripped off the tape and reconstituted into a conventional digital form for numerical processing.

The PAPA is a highly linear detector with a very large dynamic range. Unlike other 2-D photon detectors, the data rate and resolution are independent of the image intensity distribution. The major problem with the PAPA is that aberrations in the optics cause errors in the detected photon positions which are dependent on the position in the field. This shows up as a weak tartan-like pattern in the background. Recording of data with uniform illumination allows flat field corrections of the data that essentially eliminate all traces of the background errors. Details of the flat fielding procedure are given in section 2.3.

## 2.2 RECORDING REQUIREMENTS

Stellar speckle data recorded to be reduced using K-T have, in almost all respects, the same requirements as those for standard speckle interferometry. The key requirements are

- Short exposure times which "freeze" the atmospheric turbulence. With the PAPA detector, the time of arrival of each event is recorded, so photons may be grouped into frames in a way which maximizes the signal-to-noise ratio in the integrated power spectrum. Tests are usually run on comparison star data at a series of "exposure" times, and the signal-to-noise calculated at several frequencies in the power spectrum.
- Diffraction Sampling. Magnifying optics are used in front of the camera to rescale the image so that there are at least 2 (and preferably 3) pixels for each telescope diffraction element.

- Dispersion Correction. Counter-rotating computer controlled dispersion correcting prisms are used to compensate for the atmospherically induced dispersion at zenith angles larger than a few degrees.
- Isoplanatism. The processed field size must be small enough so that the atmosphere-telescope point spread function is invariant over the entire field.
- Spectral Bandpass. The bandpass must be narrow enough to provide temporal coherence over the whole image plane. A good rule of thumb requirement is that  $\text{Bandpass} = 1000\text{\AA}/(S \cdot D)$  where S is the seeing in arcseconds and D is the telescope diameter in meters.
- Seeing. One requirement for Knox-Thompson that is not required for speckle interferometry is that the diameter of the seeing disk be less than 1/2 the field size, since this sets the scale of phase differences in the K-T implementation. In addition, the number of frames required for a given signal-to-noise ratio increases as the 4th power of the seeing, so good seeing is imperative for good results.
- Photon noise limited detection. Correction for the photon noise bias is a crucial step in the implementation of K-T. The PAPA detector and other detectors like it are critical in allowing exact estimation and correction of these biases, unlike other 2-D analog cameras.

### 2.3 FLAT FIELDING

The procedure for flat fielding the data is to first generate a flat field "mask" using a combination of "white-field" data (in which the camera is looking at the dome or an internal uniform source) and a filtered version of the long-exposure image of the object being flat fielded (Ebstein, 1987a). Use of the object data itself allows for any dynamic changes in the flat field and reduces the requirement of recording "white-field" data to about once per night. The synthesized flat field is then applied to each frame, after the photon addresses have been binned into individual frames. One ends up with frames in which each photon is given a fractional height proportional to the flat field amplitude at that position. The steps in the operation are

1. Integrate the "white field" data into a long exposure and low pass filter with a cutoff frequency of  $\lambda / r_0$  to eliminate the high frequencies in this image,
2. Generate the long exposure of the object using direct integration of the photon data.
3. Divide the object long exposure (step 2) by a low pass filtered (cutoff =  $\lambda / r_0$ ) version of the object long exposure. This operation eliminates the object related low frequencies from the result.
4. Multiply the white field image by the result of the division performed in step 3.
5. Take the inverse of the result of step 4 and then apply a border mask which rolls off the region near the edges where there is a low signal-to-noise ratio.

6. In composing frames from the photon address data, replace each photon with the value of the flat field at that address.

The corrected frames then have the form

$$I(r) = \sum_j FF(r_j) \delta(r - r_j)$$

where  $FF(r_j)$  is the flat field.

### 3. The Knox-Thompson Algorithm

#### 3.1 SPECKLE INTERFEROMETRY

Short exposure images recorded in the image plane of a large telescope have the form

$$I(r) = O(r) \otimes S(r) \quad 3.1$$

where  $I(r)$  is the image,  $O(r)$  is the object intensity distribution and  $S(r)$  is the telescope-atmosphere point spread function.  $\otimes$  represents the convolution operation.

Fourier transforming

$$\hat{I}(f) = \hat{O}(f) \cdot \hat{S}(f) \quad 3.2$$

Here  $\hat{O}(f)$  is the object spectrum and  $\hat{S}(f)$  is the transfer function. In conventional speckle interferometry, the ensemble averaged power spectrum is obtained for a large set of short exposure images

$$\langle |\hat{I}(f)|^2 \rangle = |\hat{O}(f)|^2 \cdot \langle |\hat{S}(f)|^2 \rangle \quad 3.3$$

Here  $\langle \rangle$  indicates the ensemble average and  $|\cdot|$  the modulus.

#### 3.2 KNOX-THOMPSON IN FOURIER SPACE

In the Knox-Thompson process we save three quantities

$$\langle A(f) \rangle = \langle |\hat{I}(f)|^2 \rangle - \langle \sum_j FF^2(r_j) \rangle \quad 3.4$$

$$\begin{aligned} \langle \hat{D}_u(f) \rangle &= \langle \hat{I}^*(f) \hat{I}(f + \Delta f_u) \rangle \\ &= \langle |\hat{I}(f)|^2 \rangle \cdot \langle \exp\{-i[\phi(f) - \phi(f + \Delta f_u)]\} \rangle \\ &\quad - \langle \sum_j FF^2(r_j) \cdot \exp(i[\Delta f_u f_j]) \rangle \end{aligned} \quad 3.5$$

$$\begin{aligned}
 \langle \hat{D}_v(f) \rangle &= \langle \hat{I}^*(f) \hat{I}(f + \Delta f_v) \rangle \\
 &= \langle |\hat{I}(f)|^2 \rangle \cdot \langle \exp(-i[\phi(f) - \phi(f + \Delta f_v)]) \rangle \\
 &\quad \cdot \langle \sum_j F F^2(f_j) \cdot \exp(i[\Delta f_v f_j]) \rangle
 \end{aligned} \tag{3.6}$$

The quantity in equation 3.4 is the conventional result of speckle interferometry, photon noise bias corrected power spectrum. After ensemble averaging, the power spectrum may be Fourier transformed back to image space, producing an autocorrelation with centro-symmetry. While information such as binary separations, position angles and relative intensities of the components can be extracted from the autocorrelation, in many cases important information is lost, particularly for complex extended objects. The two additional terms saved in the K-T process are given in equations 3.5 and 3.6. They represent the complex autocorrelation where  $\Delta f_u$  and  $\Delta f_v$  are small (compared to the atmospheric correlation length,  $r_0$ ) constant displacements in Fourier space.

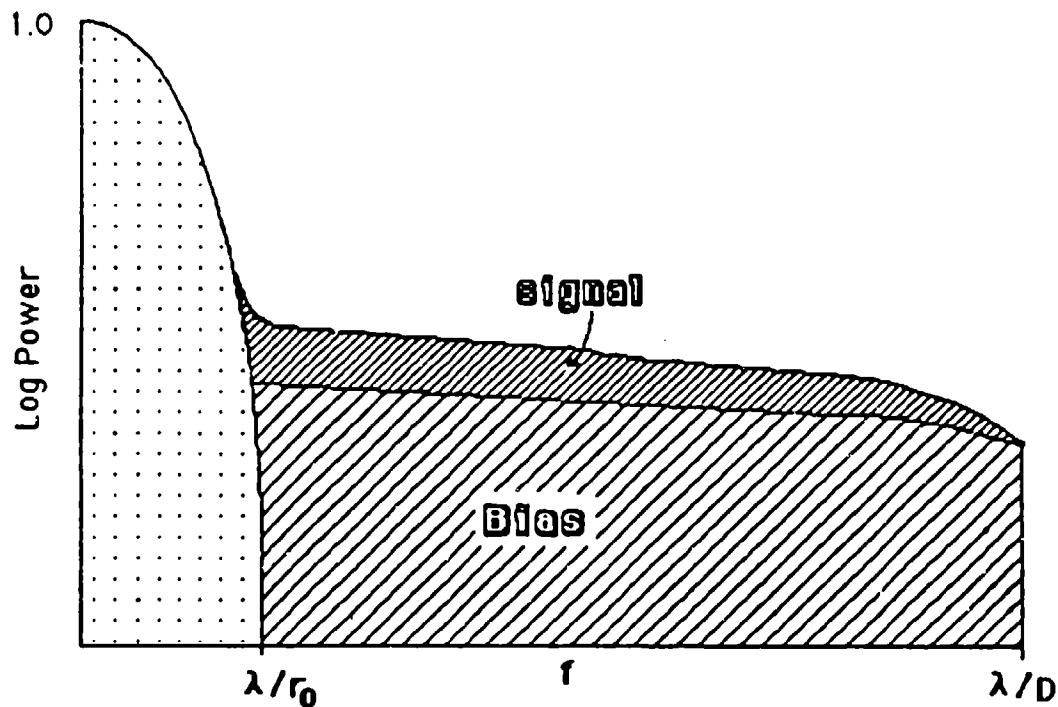


Figure 2. Speckle Transfer Function + Photon Noise Bias

Two crucial steps in the implementation of K-T are the precise correction of the photon noise biases and the correction for the speckle transfer function. The reasons for this are demonstrated in figure 2. For faint objects, the relatively small signal sits on a huge bias which must be subtracted for an accurate reconstruction. If the photons are not delta functions, the bias will have a shape which must be accurately known. Equivalent bias adds large phase errors to the cross spectrum terms and severely degrades the reconstructed phases. Since most of the power in the speckle power spectrum is located at frequencies below  $\lambda/r_0$ , the long exposure cutoff, accurate estimation of the transfer function must be made from comparison star data. Small changes in  $r_0$  between the recording of the object and the comparison star will yield large errors in amplitude calibration.

The photon noise bias is easily corrected for data from a photon counting camera such as the PAPA, since the photon count is exactly known, and the centroid of each photon image is detected as a delta function (unlike analog cameras where a photon image spreads over several pixels and the photon count may only be estimated). When the frames are flat fielded and the photons are no longer unit amplitude, the bias correction terms are derived by first integrating the square of the long exposure image. The Fourier transform of this image is then evaluated at  $f = 0$ ,  $f = \Delta f_u$  and  $f = \Delta f_v$ . These quantities are then subtracted from the corresponding integrated power and cross spectra, as indicated in equations 3.3 to 3.5.  $\hat{D}_u$  and  $\hat{D}_v$  may be expanded. For example

$$\begin{aligned} \langle \hat{D}_u(f) \rangle &= \hat{O}(f) \cdot \hat{O}(f + \Delta f_u) \cdot \exp\{i[\phi(f) - \phi(f - \Delta f_u)]\} \\ &\times \langle \hat{T}(f) \cdot \hat{T}(f + \Delta f_u) \rangle \cdot \langle \exp\{i[\Psi(f) - \Psi(f - \Delta f_u)]\} \rangle \end{aligned} \quad 3.7$$

But  $\langle \hat{T}(f) \cdot \hat{T}(f + \Delta f_u) \rangle = \langle |\hat{T}(f)|^2 \rangle$  which is just the speckle interferometry transfer function, a quantity which may be estimated from an unresolved star close in angular position to the object, and  $[\Psi(f) - \Psi(f - \Delta f_u)]$  is the atmospheric phase difference, which is a mean zero stochastic process, if the telescope adds no asymmetric aberrations. Therefore, after averaging we are left with two complex arrays which are weighted by the speckle transfer function and which contain phase difference information in the  $u$  and  $v$  directions. We will use the power spectrum data to extract the amplitudes of the image Fourier transform and these phase difference arrays to recover the image phase.

After averaging, we extract phases from the  $\hat{D}_u$  and  $\hat{D}_v$  arrays using an iterative least squares approach. The details of the phase recovery process are discussed in section 3.5

### 3.3 KNOX-THOMPSON IN IMAGE SPACE

Data recorded in a photon counting mode may easily be integrated in image space using the photon coordinates. This is advantageous for the implementation of real-time correlators and even for some computation schemes. The computation time

required to perform the image plane correlation increases as the square of the number of photons, while the Fourier transform is performed frame by frame, even when the frame is nearly empty. Therefore, depending on the processor, the image plane operation will be more efficient for small numbers of photons/frame (usually on the order of a few hundred to a thousand) while an FFT will be better at higher light levels.

Again, three quantities are ensemble averaged, this time in image space

$$\langle A(r) \rangle = \left\langle \sum_{nn'} \delta(r_n - r_{n'} - r) \right\rangle \quad 3.8$$

$$\langle K_u(r) \rangle = \left\langle \sum_{nn'} \delta(r_n - r_{n'} - r) \cdot \exp(-i\Delta_u \cdot r_{n'}) \right\rangle \quad 3.9$$

$$\langle K_v(r) \rangle = \left\langle \sum_{nn'} \delta(r_n - r_{n'} - r) \cdot \exp(-i\Delta_v \cdot r_{n'}) \right\rangle \quad 3.10$$

In this case, no bias terms are accumulated if we simply discard all the self-correlation terms ( $n=n'$ ), so no bias correction is needed. The complex arrays may be saved as real and imaginary arrays, requiring only a look-up table having  $n$  values (where  $n$  is the array dimension) for the complex coefficients.

Fourier transforming these quantities after the ensemble average converts them to be equivalent to the Fourier integration results, allowing the phase and amplitude reconstruction procedures described in sections 3.4 and 3.5 to be applied.

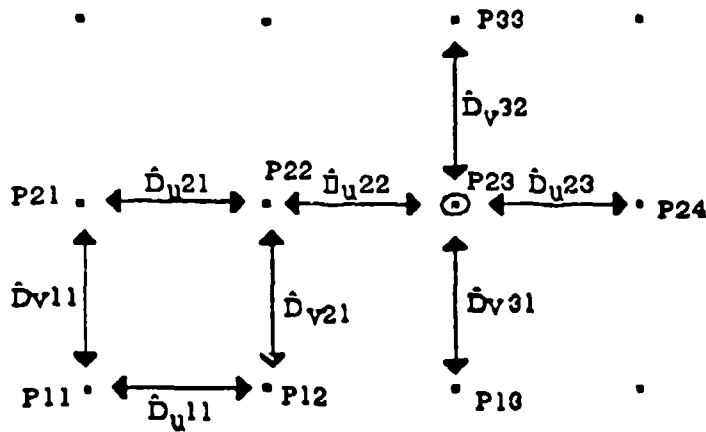
### 3.4 AMPLITUDE RECONSTRUCTION

If speckle data is recorded for an unresolved star as well as for the object, the comparison star data may be used to correct the speckle transfer function. In general, the comparison star is chosen to be as close in angular position to the object as possible. Data sets on the comparison star are taken interspersed with data on the object so that seeing changes are minimal. We have found that taking 5 minutes of data on the comparison star, then 10 minutes on the object, and then 5 minutes on the comparison star again is about optimal in terms of efficient use of telescope time and minimizing seeing changes.

In the data processing, the comparison star data is integrated using the same procedures for the object. The last operation in the reconstruction procedure is to divide the amplitudes from the object spectrum by the amplitudes from the comparison star. A similar operation is used to correct the object phases using the comparison star reconstructed phases. The corrected amplitudes are then rolled off using a low pass filter (usually in the form of an "optimum" filter which minimizes sidelobes in the image).

### 3.5 PHASE RECONSTRUCTION

The scheme for phase reconstruction from the complex cross spectrum is shown in figure 3. The procedure for phase recovery consists of setting one point (usually the  $f = 0$  point) equal to unit amplitude and zero phase. First estimates for the phasors along the first row and first column are then calculated as the product of the phasor at



1st Estimate:

$$P_{11} = 1;$$

$$P_{12} = \hat{D}_{u11} \cdot P_{11} / |P_{12}|$$

$$P_{22} = (\hat{D}_{v21} \cdot P_{12} + \hat{D}_{u11} \cdot P_{11}) / |P_{22}|; \text{etc}$$

Iteration Example:

$$P_{23} = [\hat{D}_{u23}^* \cdot P_{23} + \hat{D}_{v32}^* \cdot P_{33} + P_{33} + \hat{D}_{u22} \cdot P_{22}]$$

$$+ \hat{D}_{v31} \cdot P_{13}] / |P_{23}|; \text{etc}$$

Figure 3. Phase Integration Procedure

the previous point multiplied by the appropriate  $\hat{D}_u$  or  $\hat{D}_v$  term, normalized back to a phasor. Use of the complex amplitude in the phase integration produces a natural weighting of the phase reconstructor, proportional to the signal along that path. The interior points are then calculated using a two term average. See for example the calculation for  $P_{22}$  in Figure 3. These operations provide a fairly crude first estimate of

the phase, leaving large cumulative errors at higher frequencies (further away from  $f=0$ ). This error is then redistributed over the entire frequency plane using an iterative algorithm which converges to a result equivalent to the least squares solution for the phasors. The iteration is demonstrated in figure 3 to obtain a new estimate of P23. The iteration starts at the  $f = 0$  point and works its way out to the maximum frequency following a spiral path. Successive clockwise and counter-clockwise spiral paths are followed. The iteration continues until a stable solution is reached, usually between 20 to 100 cycles. The resulting phasors are corrected for the effects of asymmetric telescope aberrations by a division with the reference star phasors. The final reconstructed phasors are then multiplied by the deconvolved amplitudes and Fourier transformed back to image space to produce an image.

### 3.6 EXTENDED KNOX-THOMPSON

Improved signal-to-noise can be obtained with K-T by calculating additional complex cross spectrum arrays for other scales of  $\Delta f_x$  and  $\Delta f_y$ . These phasor estimates may then be averaged with the original estimates, using a weighting proportional to the degree of atmospheric correlation at those spacings. In general, only a few additional terms contribute to improved signal-to-noise, since except under extremely good conditions, the atmospheric correlation drops rapidly to zero at larger separations. The diagonal terms add most of the additional information.

### 3.7 CLEANUP ALGORITHMS

Several algorithms are available for "cleaning up" the images after the K-T reconstruction. These include Fienup, Constrained Iterative Algorithm (CIA), Iterative Deconvolution, and Maximum Entropy. Some success has been obtained with all of them, however they are all non-linear, so while they may improve the image morphology, they do not appear to preserve the accuracy of the amplitudes. The original reconstructions (and for simple objects, the autocorrelation images) seem to give the most accurate amplitude estimates. A summary of the algorithms and their uses follows:

- The Fienup algorithm (Fienup, 1978) applies image plane constraints including positivity and finite support to adjust the phases while keeping the original amplitudes. This algorithm was originally suggested for obtaining phases when only the amplitudes are known. Starting with the K-T phase estimates and high signal-to-noise deconvolved amplitudes, this technique usually converges in a few cycles, reducing background with little effect on the photometric accuracy. The success of the procedure is highly dependant on the signal-to-noise in the amplitude spectrum.
- Constrained Iterative Algorithm (CIA) is designed to clean up the amplitudes by applying a set of image and Fourier plane constraints (Ebstein, 1987b). Iteration between Fourier space and Autocorrelation space constrains the deconvolution to be between signal-to-noise bounds, and the autocorrelation to be positive and to have a finite support. This algorithm is effective for improving noisy amplitudes, but it can produce spurious peaks in the image and does not preserve amplitude ratios with great accuracy.

- Iterative Deconvolution (Ayers and Dainty 1988) iterates between new estimates of the image and of the point spread function using similar image plane constraints as Fienup. This approach appears to produce very clean deconvolutions, with no side band problems. Its linearity is untested at this time.
- Maximum Entropy (MEM) Many different implementations of maximum entropy have been introduced. This technique has proven to be very successful for improving radio maps. Again this technique has been reasonably successful at cleaning up when good estimates of the images are provided from K-T. However, accurate amplitude ratios do not appear to be preserved.

### 3.8 CONVERGENCE

The convergence of the phase from the K-T integration may be calculated (Nisenson and Papaliolios, 1983) in a manner very similar to the calculation for the amplitudes (Goodman and Belsher, 1976). The approach is to calculate the variance of the complex autocorrelation. For example, the variance for  $\hat{D}_u(f)$  is given by

$$\sigma^2(f) = \langle |\hat{D}_u(f)|^2 \rangle - |\langle \hat{D}_u(f) \rangle|^2 \quad 3.11$$

From this analysis, we can show that the number of frames required for convergence,  $M$ , is related to the number of detected photons,  $P$ , the number of speckles in the seeing disk,  $n_s$ , the object spectrum,  $\hat{O}$ , and the allowed phase error,  $\epsilon$ , at the spatial frequency  $f/f_{\max}$  where  $f_{\max}$  is the frequency cutoff (usually the telescope diffraction limit). Then

$$M \geq \frac{1}{2 \left[ \frac{P}{n_s} (1-f/f_{\max}) \cdot \hat{O}(f) \cdot \epsilon \right]^2} \quad 3.12$$

A reasonable requirement for convergence is to choose  $\epsilon$  to be  $1/10 \lambda$  at a frequency of 0.9 (90% to the diffraction limit), then

$$M = 125 \cdot \left[ \frac{P}{n_s} \right]^{-2} \quad 3.13$$

where  $n_s = 2 \cdot (D/r_0)^2$

We point out that the number of frames required for convergence increases as the 4th power of the seeing ( $r_0$ ). It is obvious that the magnitude limit of the process is highly dependent on the quality of the seeing.

As an example, with a 13th magnitude star we detect 10000 photons per second with a 4-meter telescope, an overall detection efficiency of 5% (optical and quantum), and 1 arcsecond seeing ( $r_0 = 10$  cm). Then we will have about 3700 speckles and we find for  $M$  from equation 3.15:  $M = 170,000$  frames or 1/2 hour observation with a full duty cycle camera. Of course, even for faint objects, substantial enhancement can be

obtained at lower spatial frequencies. The real criteria are set by the specific scientific goals of a given program.

### 3.9 KNOX-THOMPSON MISCONCEPTIONS

The original implementation of K-T (Knox, 1976) had many problems when it was applied to real noisy data. Knox averaged phases differences (rather than vector differences). This many times resulted in  $2\pi$  ambiguities in the average. Zeroes in the object transform yield indeterminate phases and phase differences and a breakdown in the phase integration process. In addition, the step of integrating from phase differences to phases was performed by a simple summing process from low to high frequencies, resulting in an integrated error at the higher frequencies. Finally, Knox believed that centroiding was necessary for each image before integration, adding to the computation time and increasing the error for faint objects due to poor centroiding caused by photon noise.

In the CfA implementation of Knox-Thompson, the problems of  $2\pi$  ambiguities and transform zeroes are eliminated by averaging and integrating complex vector differences, rather than phase differences. The iterative least squares integration described in section 3.5 distributes the errors due to noise over the entire frequency plane. It averages over all phase paths with a weighting proportional to the integrated amplitude along that path. In general, the reconstructed phase will have an even better accuracy than the vector differences, since many different estimates along many independent (or partially independent) paths are averaged, reducing the error. It should be pointed out that this iterative technique can also be used for one-dimensional data, though it will only distribute the error over all frequencies (in the least squares sense), not reduce the total error, since in this case there is only one path for the integration. Finally, it is easy to show that poor centroiding results in a scalar error in the vector differences which averages independently. This error may be accurately estimated from the direct sum of the input frames and then removed from the vector differences in the ensemble, before the phase integration step.

One other misconception about K-T is that it is sensitive to telescope aberrations. It has been shown (Barakat and Nisenson, 1981) that K-T is only sensitive to odd order aberrations (e.g. coma) and not to defocussing, astigmatism, spherical, etc., and that the residual effects of the aberrations may be calibrated out using comparison star data recorded through the same optical system.

## 4. Summary

Application of the PAPA detector and speckle imaging algorithms at CfA have proceeded from a development phase to a productive scientific program. The tools available will continue to improve, both on the analytic side and in the capability of the hardware. However, our current program has produced extensive scientific results on a range of astronomically interesting problems including supergiants (Karovska, et al, 1986a), Young Stellar Objects (Nisenson et al, 1985), the supernova SN1987A (Nisenson et al, 1987, Karovska et al, 1988), Mu Cas (Karovska et al, 1986b) and Seyfert nuclei (Ebstein et al, 1989). The crucial component appears to be the availability of a good detector that is photon noise limited, for which the photon noise biases in the reconstruction processes can be accurately corrected.

The author wishes to acknowledge the many contributions made to the speckle imaging program at CfA by Costas Papaliolios, Steven Ebstein, Margarita Karovska, Robert Stachnik, Robert Noyes, Clive Standley, Laurent Koechlin, Nathaniel Carleton, and many other students and interested colleagues.

## References

- Ayers, G.R. and Dainty, J.C. 1988, *Optics Letters*, **13**, 457.  
Barakat, R. and Nisenson, P. 1981, *J.O.S.A.*, **71**, 1390.  
Ebstein, S.M. 1986, *Rev. Sci. Instrum.*, **54**, 883.  
Ebstein, S.M. 1987a, *Speckle Imaging of Active Galactic Nuclei: NGC 1068 and NGC 4151*, Ph. D. thesis, Harvard University.  
Ebstein, S.M. 1987b, *Appl. Opt.*, **26**, 1530.  
Ebstein, S.M., Carleton, N.P., and Papaliolios, C. 1989, *Ap. J.*, **346**, accepted for publication.  
Fienup, J.R. 1978, *Opt. Lett.*, **3**, 27.  
Goodman, J.W. and Belsher, J.F. 1976, *Proc. SPIE*, **75**, 141.  
Karovska, M., Nisenson, P. and Noyes, R. 1986a, *Ap. J.*, **308**, 260.  
Karovska, M., Nisenson, P. and Stachnik, R.V. 1986b, *Astron. J.*, **92**, 4.  
Karovska, M., Koechlin, L., Nisenson, P., Papaliolios, C. and Standley, C. 1988, *Ap. J.*, accepted for publication.  
Knox, K.T., 1976, *J.O.S.A.*, **66**, 1236.  
Nisenson P. and Papaliolios, C., *Opt. Comm.*, 1983, **47**, 91.  
Nisenson, P., Stachnik, R.V., Karovska, M. and Noyes, R. 1985, *Ap. J. (Letters)*, **297**, L17.  
Nisenson, P., Papaliolios, C., Karovska, M., and Noyes, R. 1987, *Ap. J. (Letters)*, **320**, L15.  
Papaliolios, C., Nisenson, P. and Ebstein, S. 1985, *Appl. Opt.*, **24**, 285.